Numerical and Experimental Investigation of Aircraft Panel Deformations during Riveting Process

G F Abdelal, G Georgiou, J Cooper, A Robotham, A Levers, P Lunt

In collaboration with Airbus-UK, the dimensional growth of aircraft panels while being riveted with stiffeners is investigated. Small panels are used in this investigation. The stiffeners have been fastened to the panels with rivets and it has been observed that during this operation the panels expand in the longitudinal and transverse directions. It has been observed that the growth is variable and the challenge is to control the riveting process to minimize this variability. In this investigation, the assembly of the small panels and longitudinal stiffeners has been simulated using static stress and nonlinear explicit finite element models. The models have been validated against a limited set of experimental measurements; it was found that more accurate predictions of the riveting process are achieved using explicit finite element models. Yet, the static stress finite element model is more time efficient, and more practical to simulate hundreds of rivets and the stochastic nature of the process. Furthermore, through a series of numerical simulations and probabilistic analyses, the manufacturing process control parameters that influence panel growth have been identified. Alternative fastening approaches were examined and it was found that dimensional growth can be controlled by changing the design of the dies used for forming the rivets.

1 Introduction

Aircraft wings are typically composed of spars (longitudinal members) and ribs (transverse members) covered by skin panels. In this study, the focus has been on skin panels made of aluminum alloy and stiffened by longitudinal stringers, which are fastened to the skin panels with rivets. During the riveting cycle, clamps are applied to the skin-stringer assembly at predefined locations, a hole and countersink is drilled, the slug rivet inserted and formed, and the formed rivet head is milled flush with the panel surface. Each rivet is formed when head and the tail dies are forced together. The time to carry out the forming procedure can be as short as 3 ms, during which time large plastic deformations of the slug rivet are experienced that create significant localized heating of the rivet material and high strain rates of around 10^3 s^{-1}.

The large diametrical expansion of the slug rivet creates a residual compressive stress field in the adjacent material around the hole, improving the fatigue life and the fluid retention of the joint. Usually, the rivet joint quality is affected by many parameters, such as plate thickness, rivet diameter, rivet pitch, and squeeze force. Mülller [1] showed that the squeeze force has the most significant role, and that a properly riveted joint using a high squeeze force can have three times the fatigue life of lower squeeze force rivets. The fastening process has been investigated experimentally and numerically by many researchers [2–9]. They studied the traditional riveting process that involves drilling, insertion of a slug, and deforming it using impact force. Their work was focused mainly on how the geometrical and manufacturing parameters of the process (squeeze force, rivet type, and plate material) affect the induced residual stresses around the joint and the fatigue performance of a single rivet specimen. Boni et al. [10] studied experimentally and numerically processing techniques to improve fatigue performance of riveted joints. Lin et al. [11] proposed an efficient technique to model large aircraft assembly in finite element using assembly variation analysis followed by substructure method. This technique considers the deformations at each joint and model its effect on the whole panel. Other

researchers [12–14] studied the self-piercing riveting technique using experimental and finite element methods. The self-piercing technique is primarily used in automobile industry, yet how efficient can it be to replace the current riveting technology in aircraft industry needs more investigation.

In large aircraft skin panels where several thousand rivets are inserted, it has been observed that the skin panels can undergo expansion in the longitudinal direction as a consequence of the fastening process. Experimental testing of panel deformations under riveting process in our labs show that this panel growth is variable in nature so the challenge for manufacturing is to be able to control the production process to minimize growth. Numerical simulation methods have been used to investigate the skin panel growth due to the fastening process of multiple rivets. Static stress and explicit finite element nonlinear finite element models of the single rivet forming were initially developed and validated against experimental data. These models were then used to predict the longitudinal deformation of small panel assemblies with multiple rivets. The simulation results were compared against experimental measurements obtained from a series of small panel samples that represented a range of different panel/stiffener thicknesses and rivet types.

Alternative designs for rivet dies were examined for single and multiple rivet insertions; an alternative riveting process, which is capable of reducing the longitudinal growth of the panel, is proposed.

Finally, the manufacturing uncertainty during the riveting process was investigated on the small panel samples for different material configurations, different rivet pitch distances and variable loading conditions.

The contribution of this study is tackling an area that has not been investigated before. This study is to investigate the effect of the riveting process parameters, such as head die design, impact force, rivets pitch, and material type on the aircraft panel deformations. Some selected parameters are studied using explicit finite element model, such as head die design and impact force, while other parameters are studied using static stress finite element model. Studying the effect of the stochastic nature of selected parameters is very time consuming and requires static stress finite element model to study it. This paper is the initial step to improve riveting manufacturing process of aircraft panels by exploring the parameters design space and recommending future research to follow, i.e., manufacturing optimization.

2 Modeling and Simulation of Single Rivet Process

2.1 Static Stress Finite Element Model.

Static stress finite element models are more practical to simulate the effect of hundreds of rivets on aircraft panels' assembly, as they are less expensive than explicit finite element models. In addition, they are more efficient to use to study the stochastic nature of the riveting process as it will be shown later in the paper. A static stress finite element model for predicting the induced residual stresses due to the riveting process was created and compared against the experimental measurements conducted by Fox and Withers [15] on a single rivet sample. The modeling scheme used was based on the work of Kaniowski and Jachimowicz [16], where orthotropic thermal expansion of the rivet (axial–radial–tangential) was considered and temperature boundary conditions on the body of the rivet were applied in an effort to simulate the expansion and contraction of the rivet. The temperature boundary

conditions were specified from the work of Repetto et al. [17]. In this model, heat transfer between the rivet and the panel was not taken into account.

The single rivet sample is of 5/16 in. diameter, while the panel and stiffener thicknesses were 15 mm and 8.5 mm, respectively [15]. The rivet dimensions are shown in Fig. 1(a). The center part of the rivet is equivalent to the rivet hole dimensions, the tail part dimensions agrees to the standard 5/16 in. deformed rivet, while the head part is used to produce the squeeze effect along the rivet longitudinal axis.

The finite element model of the single rivet specimen using ABAQUS is shown in Fig. 1(b). Tetrahedral solid elements were used for the discretization of the model, where the panel, stiffener, and rivet were modeled as one part and different material type for each region was defined. The symmetry boundary conditions are applied to model only quarter of the model, while the far end plan is fixed in three directions.

The main objective of the single rivet model was to predict the stress field due to the rivet insertion by varying the applied temperature boundary conditions and the material thermal expansion coefficients. Selecting the temperature to be 270 °C and the expansion coefficients (axial–radial–tangential) to be -0.0002, 0.0001, 0.0001 1/ °C, respectively, the developed residual tangential and radial stresses are shown in Figs. 2(a) and 2(b). Direct comparison of the numerical results and experimental data presented by Fox and Withers [15] provided a level of confidence about this low-fidelity modeling approach, although there is some discrepancy between results closer to the rivet center. Yet, the running time of the static stress finite element model makes it very attractive for studying the stochastic nature of some selected parameters as dis- cussed later in this paper. The current static stress finite element model is capable of modeling residual stresses due to rivet insertion, but comes short to model the effect of head die design or the high-strain rate deformations near the rivet center or the stress wave propagation due to impact load. This shortage led to studying the effect of these parameters using explicit finite element model. It is recommended for future investigation to develop the static stress finite element model to simulate more parameters, which leads to studying the stochastic nature of more parameters.

2.2 Explicit Finite Element Model of the Single Rivet Insertion.

In an attempt to achieve a more accurate correlation with the experimental results [15], a high-fidelity finite element model, which included nonlinear material properties, nonlinear boundary conditions (contacts) and large deformations, was created. This nonlinear finite element model is shown in Fig. 3 along with the areas that are clamped during the riveting process. The single rivet sample is of 5/16 in. diameter, while the panel and stiffener thicknesses were 15 mm and 8.5 mm, respectively. The maximum tolerance between rivet diameter and panel insertion hole is used (0.08 mm). Investigating the effect on geometrical tolerance on panel deformations is not the focus of this study.

The clamping areas were constrained in x, y, and z directions, assuming that the clamping and friction force fix the assembly. The applied squeeze force is incrementally increased and decreased following a triangular form over a time of 1 ms, which reflects the duration of this process. The amplitude of the impact force applied on the head and tail die had a maximum value of 380 kN and 400 kN, respectively,

at 0.5 ms. Additionally, appropriate symmetry boundary conditions were considered and only a quarter of the small panel assembly was modeled.

Furthermore, the geometrical form of the tail die and the head die was modeled as rigid bodies and general contacts were defined between all the assembly components (rivet–dies–panel–stiffener). The model was meshed with hexagonal elements, as they are more appropriate for material forming simulations. The rivet was meshed with elements of size (0.25 mm), while the panel and stiffener volumes near the rivet were meshed with elements of size (0.5 mm). In addition, a frictionless contact between the rivet and the panel was considered, as typically rivets are coated with an anodic coating. The friction coefficient between the dies and the rivet was assumed to be (0.47) [18], while the friction coefficient between the panel and the stiffener was selected to be (1.3) [18]. Due to the lack of available material data for the airbus material used (rivet—head_die) shear friction law is excluded from this study. This will not affect the conclusion of this study, yet it is recommended to be applied for future work investigating fatigue life with respect to alternative head die designs.

The material models used in this nonlinear finite element analysis reflected the impact of the high strain rate and the heat generated in the rivet on the resultant residual stresses and the displacement wave progress. The standard stress–strain curve was not appropriate for this type of analysis to model the rivet deformations, where high strain rates were encountered. Consequently, a Johnson–Cook plasticity model was used in order to describe the nonlinear behavior of the rivet. The material type used for the rivet is an undisclosed AA2XXX alloy, similar in composition to AA2024-T3, while the material type used for the panel and stringer is undisclosed AA2XXX alloy, similar to AA2024-T351. More specifically, the Mises plasticity model with analytical forms of the hardening law and rate dependence, suitable for high-strain-rate deformation, was adopted. Johnson–Cook hardening is a particular type of isotropic hardening, where the static yield stress is assumed to be of the form

$$\bar{\sigma} = \left[A + B\left(\bar{\varepsilon}^{pl}\right)^{n} \right] \left[1 + C \ln\left(\frac{\dot{\bar{\varepsilon}}^{pl}}{\dot{\varepsilon}_0}\right) \right] \left(1 - \left(\frac{T}{T_{\mathrm{melt}}}\right)^{m} \right) \quad (1)$$

where ε^{-pl} is the equivalent plastic strain and $A, B, C, \dot{\varepsilon}_0, n$, and m are material parameters measured at or below the transition temperature (T_{trans} = 25 °C). The Johnson–Cook material parameters are listed in Table 1.

The applied squeeze force was set such that the rivet expansion at predefined locations matched manufacturing requirements. The amplitude of the squeeze force was selected to be 38 kN on the head die, while the amplitude of the force was 40 kN on the tail die. The predicted expansion of the rivet from the nonlinear finite element simulation, shown in Table 2, has excellent agreement with production requirements. The rivet expansion limits were of the order of 0.3 mm, indicating that the squeeze force applied on the dies can be reduced, leading to lower longitudinal growth.

Furthermore, the residual tangential and radial stresses (σ_{xx}, σ_{yy}) along the countersink line, which were predicted from the nonlinear finite element model, were compared against the experimental

results of the physical prototype, as seen in Figs. 4(a) and 4(b), respectively, demonstrating a high level of correlation compared to the lower fidelity model (Figs. 2(a) and 2(b)).

Different die designs were investigated using the single rivet model, in an effort to predict the effect of the die shape on residual stresses and identify the die design parameters that can be adjusted to reduce panel growth. More specifically, three designs of the head die were considered [20] and are shown in Fig. 5, while the corresponding nonlinear finite element model with the design variant no. 1 as head die is pictured at Fig. 6. The geometry of the tail die was kept constant, taking into account that the rivet tail formation has to satisfy specific dimensional requirements.

The predicted tangential and radial stresses along the countersink line for the three alternative head die designs are shown in Figs. 7(a) and 7(b), respectively. It is apparent that the stress field in the panel has higher values for the design variant no. 1, due to the fact that it has a larger contact area and tends to push the material in the radial direction causing higher radial expansion. On the other hand, the design variant no. 1 leads to less excess material and better contact between the rivet and panel. The developed stresses are lower for design variants no. 2 and no. 3 in comparison with the design variant no.1, due to the narrow contact area, which tends to push deformed material in the perpendicular direction, reducing the rivet expansion. Additionally, the design variant no. 2 generates a negative stress distribution (compressive), which leads to shrinkage of the material and lower panel growth, but takes longer from the rivet edge to decay. Furthermore, it was noticed that, for all the alternative head die designs, the stress field started at the stiffener first due to the existence of the countersink in the panel, which delays the contact between rivet and panel. Consequently, in cases where the difference in thickness between panel and stiffener is less than 5 mm, the stiffener is actually controlling the panel growth process.

The corresponding normal stresses along the countersink line for the three alternative head die designs are shown in Fig. 8. It is apparent that the compression stress wave that has been generated by design variant no. 2 has higher compressive values along the perpendicular direction, leading to higher resistance to panel growth. The squeeze force applied by the head die (0.001 s) generates a stress field that travels into the material in all directions, causing different deformation at each node along the countersink line, as shown in Fig. 9. Design variant no. 1 causes higher displacements around the rivet, but it decays quickly to match the displacement waves generated by the other design variants.

Finally, the displacement waves for design variants no. 2 and no. 3 are shown separately in Fig. 10, to highlight the importance of selecting the next rivet location with respect to the displacement wave generated by earlier installed rivet or rivets. As a result, the ideal rivet pitch distance may not be constant and an optimization process would help to identify the optimized locations of the rivets along the rivet path. Although it is recognized that due to structural requirement, the potential for this optimization may be limited in practical situations.

3 Modeling and Simulation of Multiple Riveting

The explicit finite element model of single rivet insertion was applied to a series of small panel assemblies that were manufactured with different panel and stiffener thicknesses as well as rivet

diameters. The results from the physical prototypes were examined in order to validate but also to improve the virtual riveting process.

3.1 Experimental Measurements.

A total of 18 small panel assemblies were manufactured, three samples from six discrete categories, with hole size and stack combinations as summarized in Table 3. Growth measurements were made of each panel using a co-ordinate measuring machine. Rivet pitch is determined to satisfy the following limits: distance between last rivet and panel edge has to be higher than twice the rivet diameter, while the minimum rivet pitch has to be four times the rivet diameter.

The small panel assemblies were 279 mm long, 51 mm wide with 63 mm tolerance in both directions. Six rivets were inserted into each coupon using electromagnetic riveting; the pitch between rivets was four times the rivet diameter. The control variable in the experimental riveting process is the rivet expansion limits that are defined in Table 2. The material type used for the rivet is an undisclosed AA2XXX alloy, similar in composition to AA2024-T3, while the material type used for the panel and stringer is undisclosed AA2XXX alloy, similar to AA2024-T351. The experiments were conducted on a dedicated holding fixture, which is shown in Fig. 11. The panels to be assembled are fixed on the holding fixture using two aluminum plates that applied enough pressure but allowing them to expand while resisting the applied friction force. The holding fixture is designed in a way to exclude the effect of boundary conditions on panel deformations.

Three measurements of the absolute length along the X-axis and 11 measurements of the absolute width along the Y-axis were obtained for each panel, as illustrated in Figs. 11 and 12. These measurements are performed before and following the riveting process to generate two sets of data that exclude the effects of panels are not machined (63 mm tolerance). The mean growth of the panel and the stiffener along the X-axis for all the points X1–X3 and all the test samples of each category is depicted in Fig. 13.

Additionally, the mean growth of the panel and the stiffener along the Y-axis for all the points Y1–Y11 and all the test samples of each category are pictured in Fig. 14. Inspecting the mean growth of the small panel assemblies along the X-axis and Y-axis, Figs. 13 and 14, it is apparent that the samples of categories 1-3-5 (minimum total stack for each rivet size 1/4 in.-5/16 in.-3/8 in.) present higher mean growth along X-axis for the stiffener, and more interestingly double the mean growth in comparison to the panel. However, the mean growth of the two components along Y-axis does not show similar behavior among the categories. The deformation of the panel and stiffener has approximately the same magnitude in all cases except category 1. Furthermore, the ratio of the mean growth of the panel along the X-axis for the maximum and minimum stack configurations and for each of the three rivet sizes is around 2.0, while the same ratio for the stiffener is around 1.2, except from the smallest rivet size (1/4 in.). Also, the mean growth along the Y-axis for both the components presents a uniform trend and is one order of magnitude below the mean growth along X-axis for the majority of the categories.

The measured growth of the panel along the X-axis for category 4, where the total stack is 24.37 mm thick, is double that in comparison to category 3, where the total stack is 11.08 mm thick. However, this trend is not observed for the deformation of the stiffener along X-axis or for the growth of the panel and

stiffener along the Y-axis. Also, this trend is not observed for the coupons of categories 5 and 6, where the total stack is 15.71 mm and 29.01 mm, respectively. For samples in categories 4 and 5, where the total stack is 24.37 mm and 15.71 mm, the measured growth of the panel and stiffener along X-axis is approximately the same, despite the significant difference in the total stack thickness. The corresponding growth of the components along the Y-axis presents similar values. Finally, for the small panel assemblies in categories 2 and 5, where the total stack is 17.54 mm and 15.71 mm, the observed growth of the panel and stiffener along the X-axis is almost double for category 5 in comparison to cate- gory 2, while the measured deformation along Y-axis is similar. This behavior is probably caused by the different type of rivet (1/4 in. and 3/8 in., respectively) and the different riveting parameters (pressure, multiple impacts, etc). So qualitatively, it can be concluded that the stiffener consistently expanded more than the panel in the minimum stack configuration, and transitioning from the minimum stack thickness to maximum stack thickness, the panel consistently exhibited a greater degree of expansion com- pared to the stiffener. This conclusion can be related to the face that the panel has countersunk while the stiffener has not.

3.2 Calibration Process.

A high-fidelity finite element model, which included nonlinear material properties, nonlinear boundary conditions (contacts) and large deformations, was created in an effort to study and simulate the panel growth on small panel assemblies due to the insertion of rivets. This nonlinear finite element model is shown in Fig. 15 along with the applied boundary conditions. The assembly was assumed to be com- pressed by aluminum plates with a spring mechanism on the left edge against the holding fixture, while on the right edge symmetry boundary condition was applied. An additional symmetry boundary condition was also applied at the XZ-plane of the coupon and as a result, only a quarter of the small panel assembly was modeled. The clamping force of the stand was replaced by an enforced compressing displacement and an appropriate coefficient of friction between the clamp and the assembly was applied. The finite element model resembled a small panel assembly from category-4 (Table 3), with panel thickness 15.07 mm and stiffener thickness 9.0 mm. The element size, the material properties, and the contact definitions were chosen to be similar to the single rivet finite element model described in Sec. 2.2.

During the simulation process, the boundary conditions of the assembly were adjusted in order to match the experimental results.

In particular, the value of the compression displacement between the panel and the top clapping plate was selected to be 0.027 mm. As a result, the predicted panel growth was 0.163 mm (experimental 0.17 mm) and the stiffener growth was 0.15 mm (experimental 0.15 mm). This step was performed to exclude the effect of boundary conditions in the finite element model, then other parameters will be varied and their impact on panel deformations is studied in Sec. 4.

Furthermore, it is apparent in Fig. 16 that during the rivet head deformation under impact squeeze force from the head die, an excess volume of rivet material is gathering under the head die. As the rivet head material is plastically deformed under high strain rate, it would require a higher squeeze force to deform the rivet and satisfy the rivet expansion limits as described in Table 2 (due to the hardening of the material under compression). Higher riveting impact force produces higher compression on the

panel (higher residual stresses), which in turn leads to higher longitudinal growth. Each head die design (Fig. 5) produces different rivet head deformation (material flow during deforming). Checking the stress wave results discussed in Sec. 2 (Figs. 7–10), recommends developing an experimental riveting program using different head die design. Then compare the impact of each different head die on the panel deformations.

4 Alternative Die Designs

An alternative head die design was examined for multiple rivet insertions while an alternative riveting process was also studied and compared against the original panel assembly and riveting process.

4.1 Multiple Rivet Insertions.

The effect of alternative head die designs on longitudinal growth was further investigated through two discrete manufacturing processes, which included multiple rivet insertions on the small panel assemblies. In particular, the first scenario included the replacement of the original head die by an alternative design, while in the second scenario only the tail of the rivet was deformed. The first approach was simulated using the same rivet length and squeeze forces on dies, clamping loads on the panel and boundary conditions, as in the original assembly of the small panel assembly (Sec. 3.2). The design variant no. 1 for the head die was proposed as a replacement candidate over the original geometry, the nonlinear finite element model of the coupon assembly is shown in Fig. 17. The selected die design requires lower squeeze force to deform the rivet, as the rivet material is free to deform in the transverse direction, and there is no excess material collected under the head die. Using the proposed design variant of the head die, a 6.1% reduction of the longitudinal growth was achieved. In an effort to avoid excessive deformation of the rivet head (Fig. 17), the squeeze force on the head die can be reduced by 13%, which leads to a 76.5% reduction in panel deformation, while satisfying the rivet expansion limits.

An alternative riveting method, shown in Fig. 18, was also examined [20]. Similar considerations, regarding the clamping forces of the assembly and boundary conditions, as in the original assembly (Sec. 3.2), were made. During this process, only the tail of the rivet was deformed, while the head of the rivet was kept fixed. This formation requires the head of the rivet to be manufactured prior to the riveting process in the shape of the countersink hole on the panel.

In Table 4, the rivet expansion values that were measured on the panel assembly for the alternative head die design and the alternative riveting processes are compared against the corresponding numerical results from the original assembly (Table 2). It can be seen that applying the nominal squeeze force on the tail die, a 54% reduction of the panel growth and 21% increase of the stiffener growth was observed.

The effect of alternative head die designs on longitudinal growth was further investigated through two discrete manufacturing processes, which included multiple rivet insertions on the small panel assemblies. In particular, the first scenario included the replacement of the original head die by an alternative design, while in the second scenario only the tail of the rivet was deformed. The first

approach was simulated using the same rivet length and squeeze forces on dies, clamping loads on the panel and boundary conditions, as in the original assembly of the small panel assembly (Sec. 3.2). The design variant no. 1 for the head die was proposed as a replacement candidate over the original geometry, the nonlinear finite element model of the coupon assembly is shown in Fig. 17. The selected die design requires lower squeeze force to deform the rivet, as the rivet material is free to deform in the transverse direction, and there is no excess material collected under the head die. Using the proposed design variant of the head die, a 6.1% reduction of the longitudinal growth was achieved. In an effort to avoid excessive deformation of the rivet head (Fig. 17), the squeeze force on the head die can be reduced by 13%, which leads to a 76.5% reduction in panel deformation, while satisfying the rivet expansion limits.

These numbers reflect the huge impact of head die design on final panel deformations. Performing parameter sensitivity analysis of the head die dimensions with respect to panel deformation is recommended for future work as it is not practical to perform such analysis using the explicit finite element model. If the static stress finite element model is developed to simulate plasticity deformations and relate them to the head die design parameters, it would be more practical to perform design optimization of the head die dimensions and configurations. Static stress finite element model is used in Sec. 5 to model stochastic process of selected riveting manufacturing process parameters, such as rivet pitch and assembly material type.

5   Uncertainty in the Manufacturing Process

Manufacturing uncertainty, related to variability in material properties, in applied boundary conditions from holding fixtures, in manufacturing loads as well as in environmental conditions, is not usually taken into account in tolerances specified in the manufacturing process. The stochastic nature of manufacturing processes is associated with significant increase in manpower requirements, manufacturing adjustments and delivery delays, affecting the product life cycle. In the current study, the impact of uncertainty in riveting process was investigated at the first level of the analysis test pyramid, which is widely used to categorize the testing in aircraft structures.

The variability in panel growth due to the riveting process was examined in a deterministic and stochastic way using the small panel assemblies (type 1) for different material configurations and different rivet pitch distances. The probabilistic analysis included multiple Monte-Carlo simulations and the distribution of the panel growth due to varying loading conditions was predicted.

5.1 Model Description.

The low-fidelity model of the single rivet insertion, described in Sec. 2.1, was implemented on the small panel assembly (type 1) in an attempt to predict the panel growth. The examined panel was built with panel dimensions (279 mm x 50 mm x 15 mm),   the   stiffener   (279 mm x 50 mm x 8.5 mm), and six rivets (3/8 in. diameter). Two discrete finite element models with different rivet pitch distances were generated, resembling the minimum allowable rivet pitch distance (38 mm) and the maximum rivet pitch distance (48 mm), respectively. The investigated finite element model of the small panel assembly

for the case of the minimum rivet pitch distance is depicted in Fig. 19. Tetrahedral solid elements were used for the discretization of the model, where the panel, stiffener, and rivets were modeled as one part and different material type for each region were defined.

The panel material was selected to be AA2024-T351 with Young's modulus 7.38 x 1010 N/m2, Poisson's ratio 0.33, and density 2780 kg/m3. The elastic–plastic hardening behavior was taken into account according to the stain–stress curve (LT-tension) included in Fig. 23 [21]. Two cases for the material type of the stiffener were considered. Initially, the material of the stiffener was assumed to be Extruded AA2024-T3 with Young's modulus 7 x 1010 N/m2, Poisson's ratio 0.33, and density 2780 kg/m3, while the nonlinear behavior of the material was described by the strain–stress curve (L-tension) included in Fig. 24 [15]. For the second case, the material type of the stiffener was selected to be AA2050-T84 with Young's modulus 7.6 x 10 N/m2, Poisson's ratio 0.33, and density 2780 kg/m3, while the yield and the tensile strengths were considered as 4.75 x 108 N/m2 and 5.1 x 108 N/m2, respectively. Finally, the material for the rivets was selected to be AA2017-T4.

The residual stresses around the rivets due to riveting process were generated by applying simultaneously the temperature boundary conditions at all rivets. The nonlinear finite element model was considered to be fixed at the right hand edge (Fig. 19), while the left hand edge of the assembly was constrained only along the z direction. Additionally, appropriate symmetry boundary conditions were applied and only the half of the model was simulated.

5.2 Deterministic Analysis.

The low-fidelity approximation of the riveting process, described in Sec. 2.1, was applied on the small panel assemblies (type 1) in an effort to predict the deformation for different rivet pitch distances and material configurations. Four deterministic nonlinear finite element analyses were con- ducted, considering the minimum and the maximum allowable rivet pitch distance as well as two discrete material types for the stiffener (AA2024-T3 and AA2050-T84), the calculated panel growth of the examined coupons is shown in Table 5.

The numerical results in Table 5 show that the insertion of the rivets at the maximum pitch distance is leading to higher longitudinal growth, while the selection of the AA2050-T84 as the material type for the stiffener results in lower deformation. The higher longitudinal growth in the case of the maximum rivet pitch distance can be explained by inspecting Figs. 2(a) and 2(b), and noticing that the residual stresses (tangential and radial) are decaying within a circle of 30 mm from the rivet center. As a result, in the case of two consecutive rivets, the stress fields developed around the rivets will share an overlapping region and will cancel each other (as stresses are acting in opposite directions) (Fig. 20).

5.3 Probabilistic Analysis.

Different scenarios of probabilistic analyses were conducted in an effort to identify the influence of the applied temperature conditions on the panel growth, the small panel assembly (type 1) was considered

in two separate material configurations and two rivet pitch distances. The applied temperature conditions at each rivet for all the case studies were varied following a normal distribution with mean value 250 o C and standard deviation 10%. The averaged total elongation of the coupon was measured at the edge and on the centerline. The FE model used in Sec. 2.1 is more effective in simulating and optimization of high number of rivets (>1000). So the temperature and virtual thermal conductivity along (x,y,z) were used to simulate the expansion/compression effect of each rivet on the panel. So, the temperature variation represents only variation in the riveting process parameters that may make the residual stresses different at each rivet.

At the first scenario, the material type of the panel and the stiffener was selected to be AA2024-T351 and AA2024-T3, respectively, while the minimum and maximum allowable rivet pitch distance was considered separately. 1000 Monte Carlo simulations were performed, changing independently each of the temperature conditions and the derived histograms of the probability density function are depicted at Fig. 21. The mean value of the averaged deformation was predicted to be 0.320 mm and the standard deviation was 0.014 mm for the minimum rivet pitch distance, while for the case of the maximum rivet pitch distance the averaged elongation was found to be 0.325 mm and the standard deviation was 0.019 mm.

In the second scenario, the stiffener material was selected to be AA2050-T84 and considering the minimum or the maximum allowable rivet pitch distance, the derived histograms of the probability density function are depicted in Fig. 22. The mean value of the averaged growth was 0.280 mm and the standard deviation was 0.013 mm for the minimum rivet pitch distance, while for the case of the maximum rivet pitch distance the total deformation was predicted to be 0.318 mm and the standard deviation was 0.019 mm.

Inspecting Figs. 21 and 22, it becomes apparent that the selection of the material type for the stiffener significantly influences the growth of the small panel assemblies (type 1), especially in the case of the minimum allowable rivet pitch distance. Additionally, the panels for both material configurations exhibited lower deformation for reduced rivet pitch distance due to the overlap- ping stress fields that were developed between the rivets and the cancellation of the residual stresses, as described in Sec. 5.2. For the same reason, the probability density functions in the case of the minimum rivet pitch distance presented lower standard deviations leading to better predictability of the panel growth. Finally, the higher sensitivity of the small panel assemblies with material AA2024-AA2050 to the rivet pitch distance is due to the fact that the stiffener is stiffer than the panel leading to higher cancellation of the residual stresses for reduced rivet pitch distance in comparison to the panel with material AA2024 (T351/T3).

6 Conclusions

A detailed study on the fastening process of small panel assemblies with single and multiple rivets was performed. Initially, static and explicit finite element models for approximating the riveting process on single rivet samples were created and validated against published experimental data. The induced residual stresses were found to depend upon different process parameters, such as the clamping

conditions, the squeeze forces on dies as well as the material modeling and the properties of the contacts between panel, stiffener, and rivet. Afterward, the explicit finite element model was implemented for the insertion of multiple rivets on small panel assemblies. The numerical results of the observed panel growth were calibrated using experimental measurements that were performed in VEC labs. The explicit finite element model produces more accurate results, but more expensive time- wise compared to the static stress finite element model. Yet, the applied static stress finite element model is not able to capture all process parameters, such as head die design and strain rate. Studying the mechanical and thermal effect of hundreds of rivets on aircraft panels, requires developing more accurate static stress finite element models.

Alternative die designs and a different riveting process were investigated and proposed in an attempt to reduce the panel growth. Particularly, the deformations and the residual stresses around rivets developed due to riveting process using three alternative head die designs on single rivet samples were examined. Additionally, an alternative head die design and a different manufacturing method was studied separately on process control coupons (type 1) predicting significant reduction on the panel growth, while satisfying the rivet expansion limits. Finally, a probabilistic analysis was conducted in an effort to quantify the uncertainty induced from the manufacturing process. From this analysis, it was found that the panel growth also depends upon the rivet pitch distance, the material of the stiffener as well as the manufacturing loads.

This paper is the first to investigate the panel growth of riveted assembly, and its conclusion will change the techniques, which the assembly engineers are applying to rivet panels. Future work should focus on developing more accurate surrogate model (static finite element) of the explicit finite element model and on studying the effect of different head die designs on fatigue life of riveted panels.

Nomenclature

A = Johnson–Cook material parameter (MPa)

B = Johnson–Cook material parameter (MPa)

D_n = rivet expansion

m = Johnson–Cook material parameter

n = Johnson–Cook material parameter

Tmelt = material melting temperature (o C)

ε^{-pl} = equivalent plastic strain

Appendix

Material Properties.

The strain–stress plots (Figs. 23 and 24) are represented as engineering strain versus engineering stress and Eq. (A1) is applied in order to convert the data to true strain versus true stress as well as to calculate the plastic strain–stress part, which is used in nonlinear finite element analysis

$$Truestrain = \ln(1 + Eng.strain)$$

$$Truestress = \frac{(Eng.stress)(1 + Eng.strain)}{\left(1 + (1 - 2v)\frac{Eng.stress}{E}\right)}$$

$$Plastic\ strain = True\ strain - \frac{True\ stress}{E}$$

where E and v are the Young's modulus and Poisson's ratio of the material, respectively.

References

[1] Müller, R. P. G., 1995, "An Experimental and Analytical Investigation on the Fatigue Behaviour of Fuselage Riveted Lap Joints: The Significance of the Rivet Squeeze Force and a Comparison of 2024-T3 and Glare 3," Ph.D. dissertation, Delft University of Technology, Delft, The Netherlands.

[2] Deng, X., and Hutchinson, J. W., 1998, "The Clamping Stress in a Cold-Driven Rivet," Int. J. Mech. Sci., 40(7), pp. 683–694.

[3] Langrand, B., Deletombe, E., Markiewicz, E., and Drazetic, P., 2001, "Riveted Joint Modeling for Numerical Analysis of Airframe Crashworthiness," Finite Elements in Analysis and Design, 38(1), pp. 21–44.

[4] Li, G., and Shi, G., 2004, "Effect of the Riveting Process on the Residual Stress in Fuselage Lap Joints," CASI J., 50(2), pp. 91–105.

[5] Ryan, L., and Monaghan, J., 2000, "Failure Mechanism of Riveted Joint in Fibre Metal Laminates," J. Mater. Process. Technol., 103(1), pp. 36–43.

[6] Szolwinski, M. P., and Farris, T. N., 2000, "Linking Riveting Process Parameters to the Fatigue Performance of Riveted Aircraft Structures," J. Aircr., 37(1), pp. 130–137.

[7] Rans, C., Straznicky, P. V., and Alderliesten, R., 2007, "Riveting Process Induced Residual Stresses Around Solid Rivets in Mechanical Joints," J. Aircr., 44(1), pp. 323–329.

[8] Deng, J. H., Yu, H. P., and Li, C. F., 2009, "Numerical and Experimental Investigation of Electromagnetic Riveting," Mater. Sci. Eng. A, 499(1–2), pp. 242–247.

[9] Li, G., Shi, G., and Bellinger, N. C., 2012, "Assessing the Riveting Process and the Quality of Riveted Joints in Aerospace and Other Applications," Welding and Joining of Aerospace Materials, Elsevier, Technology & Engineering, pp. 181–214.

[10] Boni, L., Lanciotti, A., and Polese, C., 2014, "Some Contraindications of Hole Expansion in Riveted Joints," Eng. Failure Anal., 46, pp. 140–156.

[11] Lin, J., Jin, S., Zheng, C., Li, Z., and Liu, Y., 2014, "Compliant Assembly Variation Analysis of Aeronautical Panels Using Unified Substructures With Consideration of Identical Parts," Comput.-Aided Des., 57, pp. 29–40.

[12] Mori, K., Abe, Y., and Kato, T., 2014 "Self-Pierce Riveting of Multiple Steel and Aluminium Alloy Sheets," J. Mater. Process. Technol., 214(10), pp. 2002–2008.

[13] Li, Y. B., Wei, Z. Y., Wang, Z. Z., and Li, Y. T., 2013, "Friction Self-Piercing Riveting of Aluminum Alloy AA6061-T6 to Magnesium Alloy AZ31B," ASME J. Manuf. Sci. Eng., 135(6), pp. 1–7.

[14] Lou, M., Li, Y. B., Li, Y. T., and Chen, G. L., 2013, "Behavior and Quality Evaluation of Electroplastic Self-Piercing Riveting of Aluminum Alloy and Advanced High Strength Steel," ASME J. Manuf. Sci. Eng., 135(1), pp. 1-9.

[15] Fox, M. E., and Withers, P. J., 2007, "Residual Stresses in and Around Electromagnetically Installed Rivets Measured Using Synchrotron and Neutron Diffraction," J. Neutron Res., 15(3-4), pp. 215–223.

[16] Kaniowski, J., and Jachimowicz, J., 2009, "Methods for FEM Analysis of Riveted Joints of Thin-Walled Aircraft Structures within the Imperja Project," Proceedings of the 25th ICAF Symposium, Rotterdam, The Netherlands, May 27–29, pp. 939–967.

[17] Repetto, E. A., Radovitzky, R., Ortiz, M., Lundquist, R. C., and Sandstrom, D.R., 1999, "A Finite Element Study of Electromagnetic Riveting," ASME J. Manuf. Sci. Eng., 121(1), pp. 61–68.

[18] ASM Handbook, 1992, Friction, Lubrication, and Wear Technology, Vol. 18, ASM International.

[19] Kay, G., 2003, "Failure Modeling of Titanium 6A1-4V and Aluminum 2024-T3 With the Johnson–Cook Material Model," Lawrence Livermore National Laboratory, Technical Report No. Dot/FAA/AR-03/57.

[20] Hartmann, J., Brown, T., Pinkerton, B., and Nixon, K., 1993, "Integration and Qualification of the HH500 Hand Operated Electromagnetic Riveting System on the 747 Section 11," SAE Technical Paper No. 931760.

[21] Niu, M. C. Y., 1988, Airframe Structural Design, Conmilit Press Ltd., Hong Kong. [22] Szolwinski, M. P., 1998, "The Mechanics and Tribology of Fretting Fatigue With Application to Riveted Lap Joints," Ph.D. dissertation, Purdue University, West Lafayette, IN.

Tables

Material type	Aluminum 2017-T4
Johnson–Cook parameters	$A = 369\,\text{MPa} - B = 684\,\text{MPa}$ $n = 0.73 - m = 1.7$ $C = 0.0083 - \varepsilon^o = 1$ $T_{\text{melt}} = 775\,\text{K}$

Table 1 material mechanical property [19]

	Rivet Expansion Finite Element Model
	$D1 = 0.560$ mm $D2 = 0.390$ mm $D3 = 0.386$ mm $D4 = 0.514$ mm
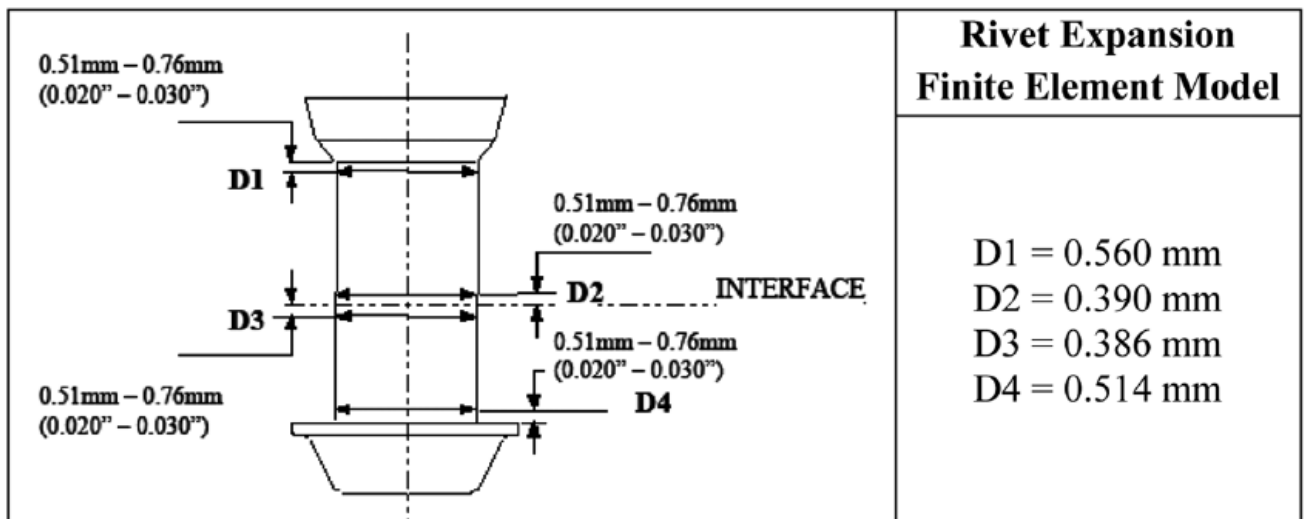
Table 2 Rivet expansion values

Cat.	Rivet pitch distance	Hole size (in.)	Panel thickness (mm)	Stiffener thickness (mm)	Total stack (mm)
1	Min	1/4	4.34	2.48	6.82
2	Max	1/4	11.16	6.38	17.54
3	Min	5/16	7.05	4.03	11.08
4	Max	5/16	15.07	9.30	24.37
5	Min	3/8	10.00	5.71	15.71
6	Max	3/8	18.46	10.55	29.01

Table 3 Stack combinations and hole size for the process control coupons (type 1)

Rivet expansion original head die	Rivet expansion alternative head die	Rivet expansion alternative process
$D1 = 0.560$ mm	$D1 = 0.340$ mm	$D1 = 0.240$ mm
$D2 = 0.390$ mm	$D2 = 0.330$ mm	$D2 = 0.270$ mm
$D3 = 0.386$ mm	$D3 = 0.342$ mm	$D3 = 0.250$ mm
$D4 = 0.514$ mm	$D4 = 0.540$ mm	$D4 = 0.540$ mm

Table 4   Rivet expansion values for alternative head die design and riveting process

Rivet pitch distance stiffener material	Minimum AA2024-T3	Maximum AA2024-T3	Minimum AA2050-T84	Maximum AA2050-T84
Panel growth (mm)	0.34	0.36	0.307	0.35

Table 5 Panel growth of the process control coupons (type 1)

Figures
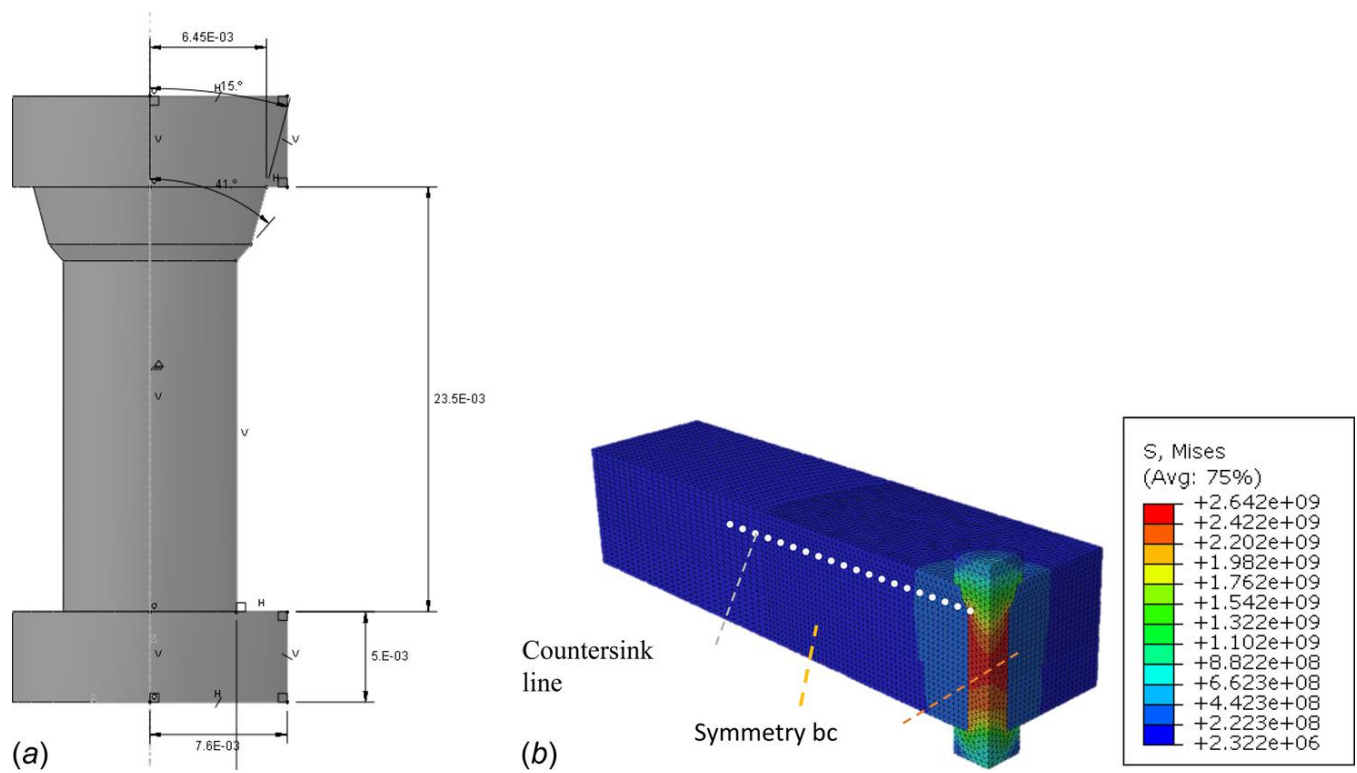
Fig. 1 (a) Deformed rivet dimensions and (b) Von Mises stress distribution on the single rivet sample along the countersink line

(a)

(b)
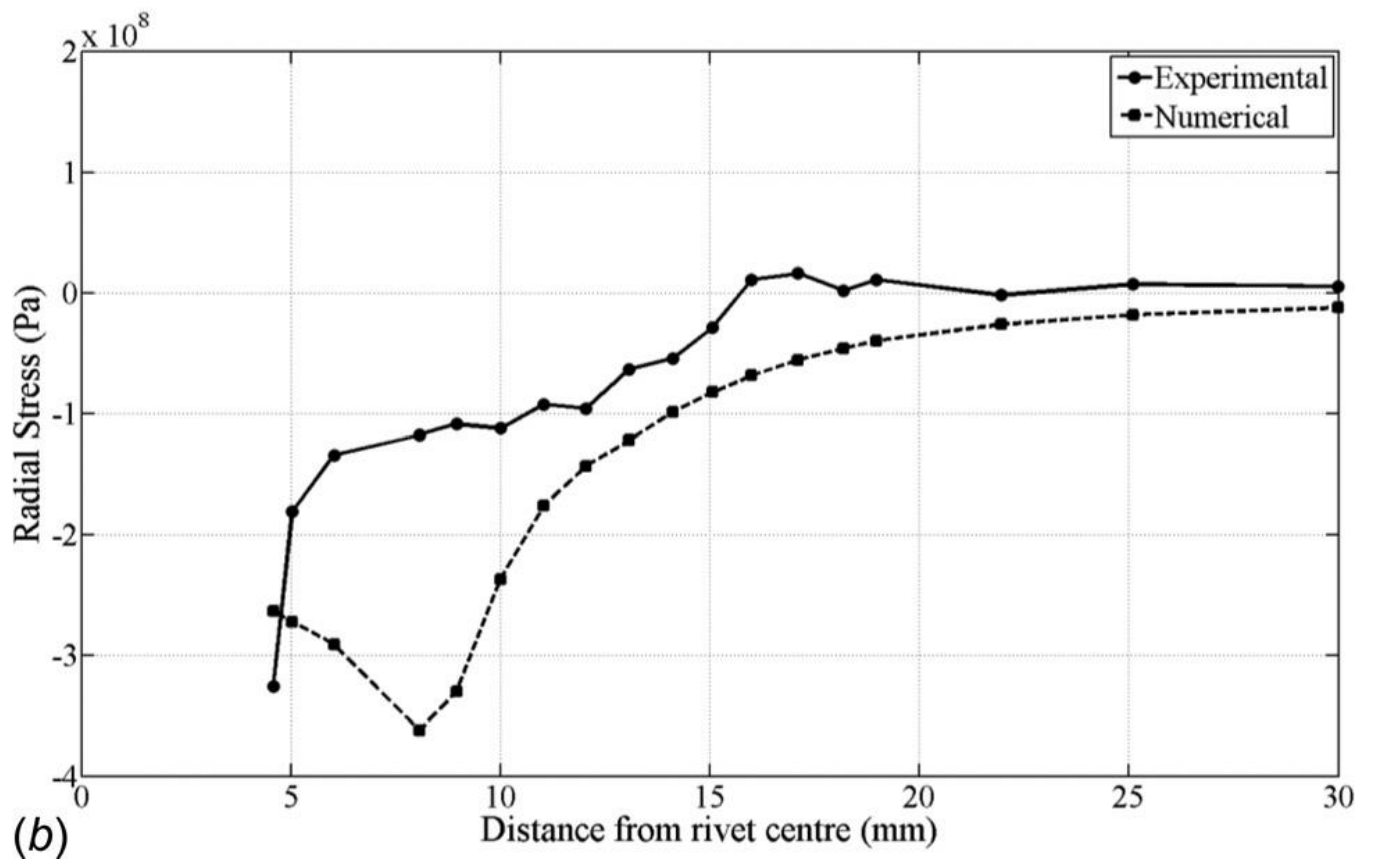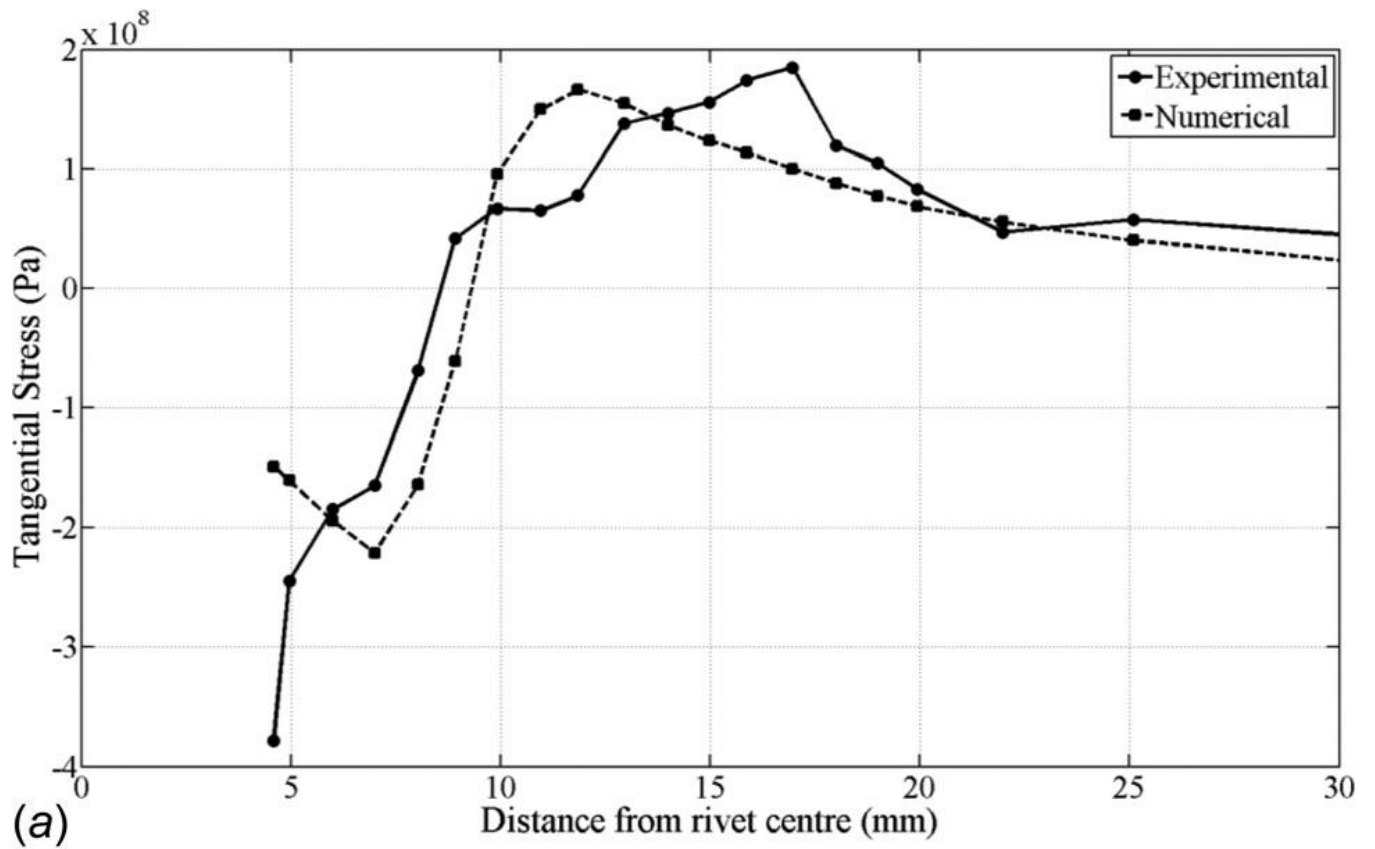
Fig. 2 (a) Numerical and experimental [15] residual tangential stresses along the countersink line and (b) radial stresses along the countersink line

Clamp Areas
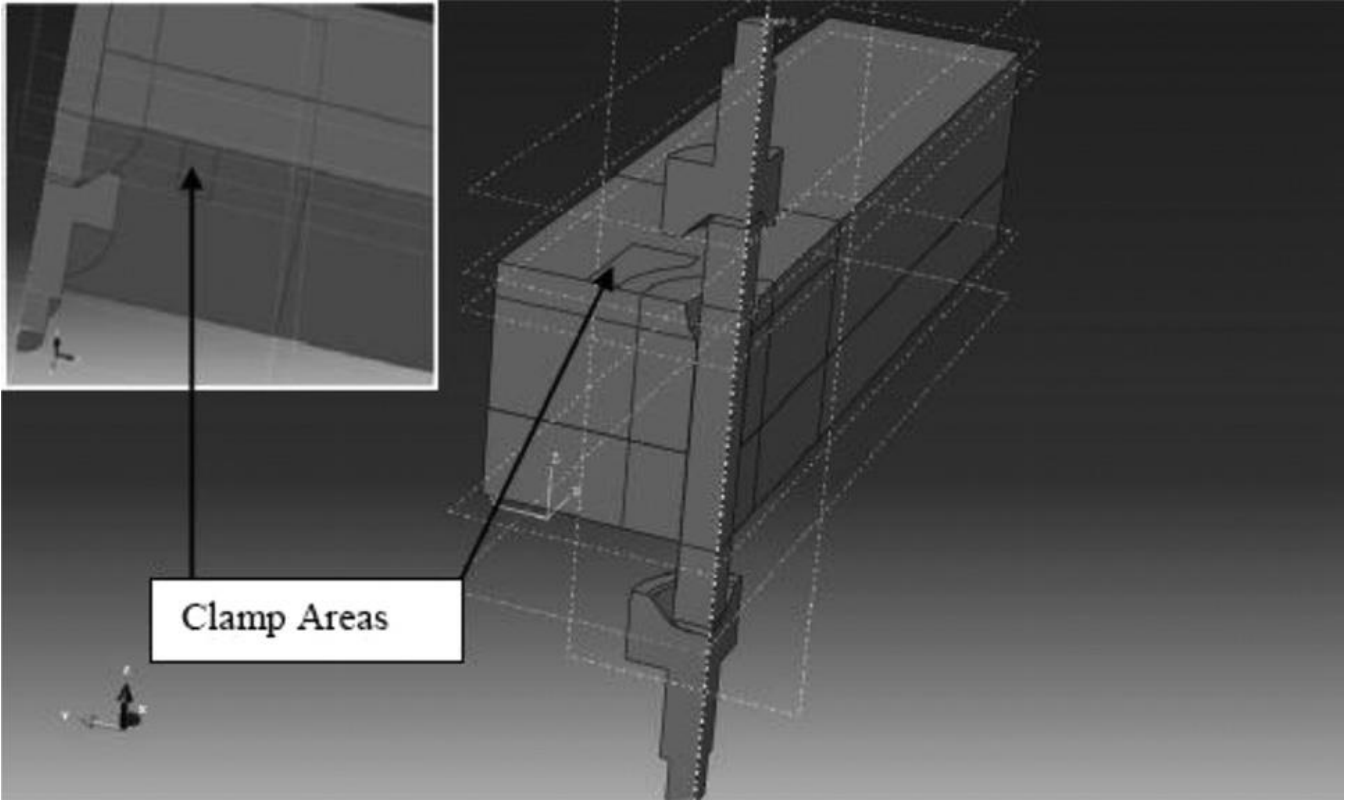
Fig. 3   Nonlinear finite element model for simulating single rivet insertion

(a)

(b)
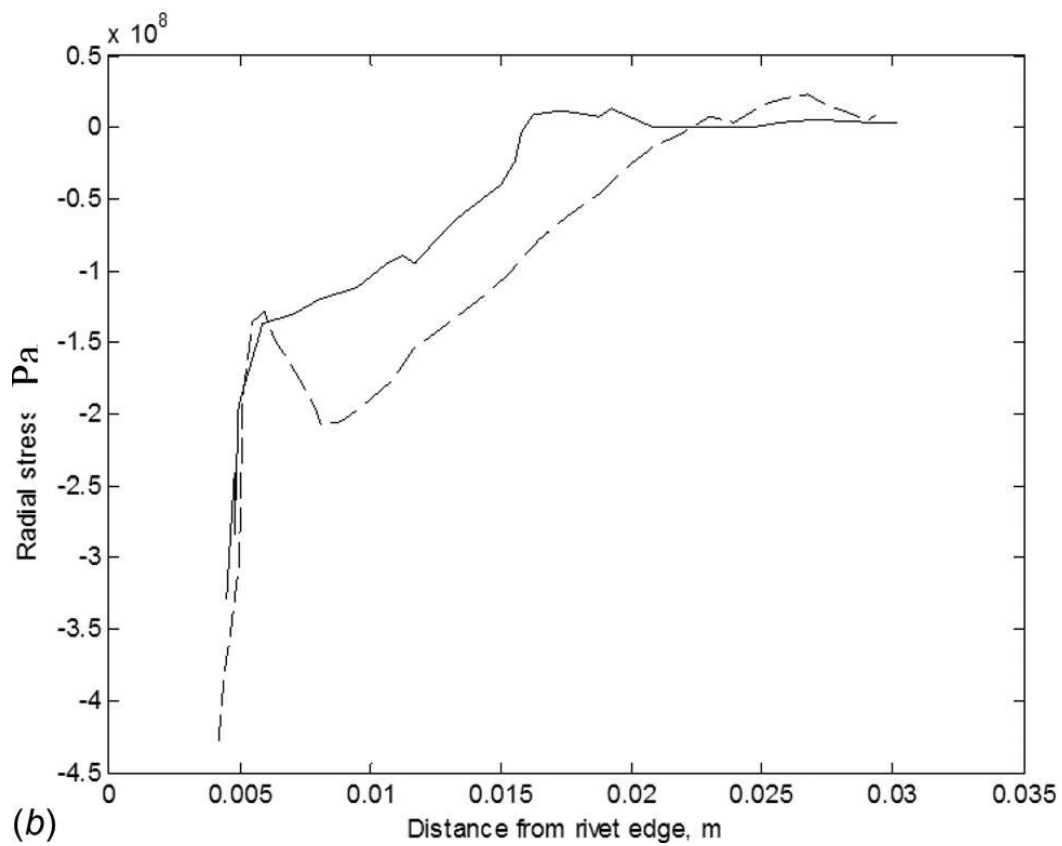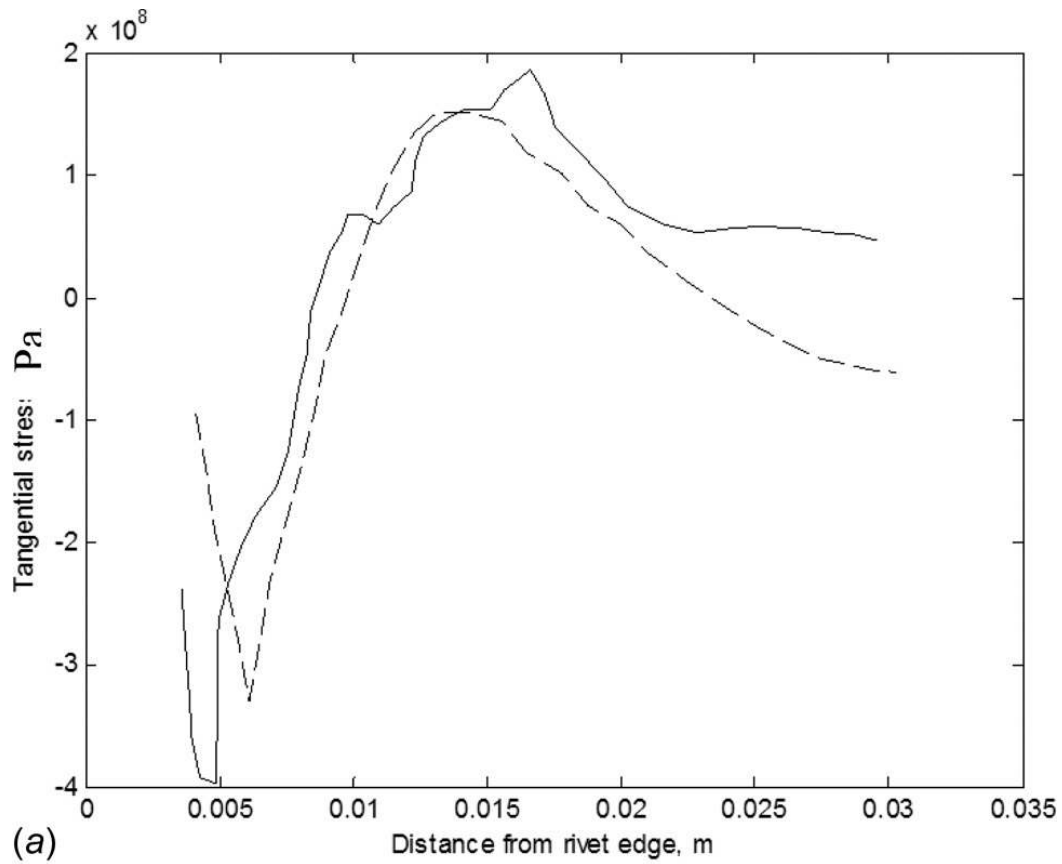
Fig. 4 (a) Numerical (dashed line) and experimental (solid line) [15] residual tangential stresses along the countersink line and (b) radial stresses along the countersink line
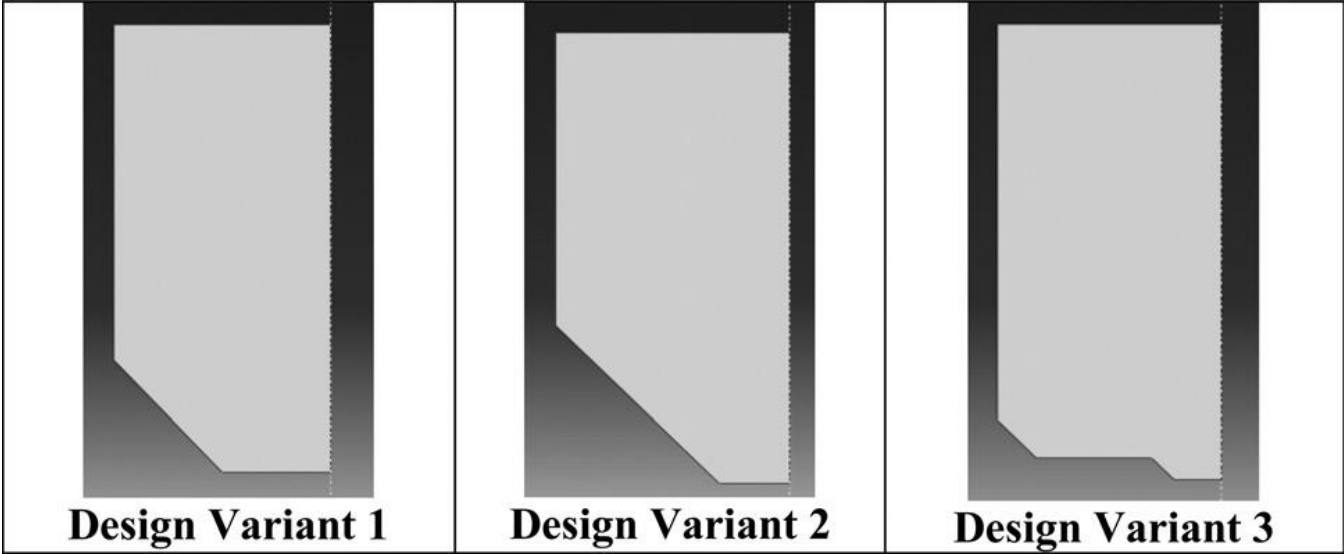
Fig. 5 Cross section of alternative head_die designs
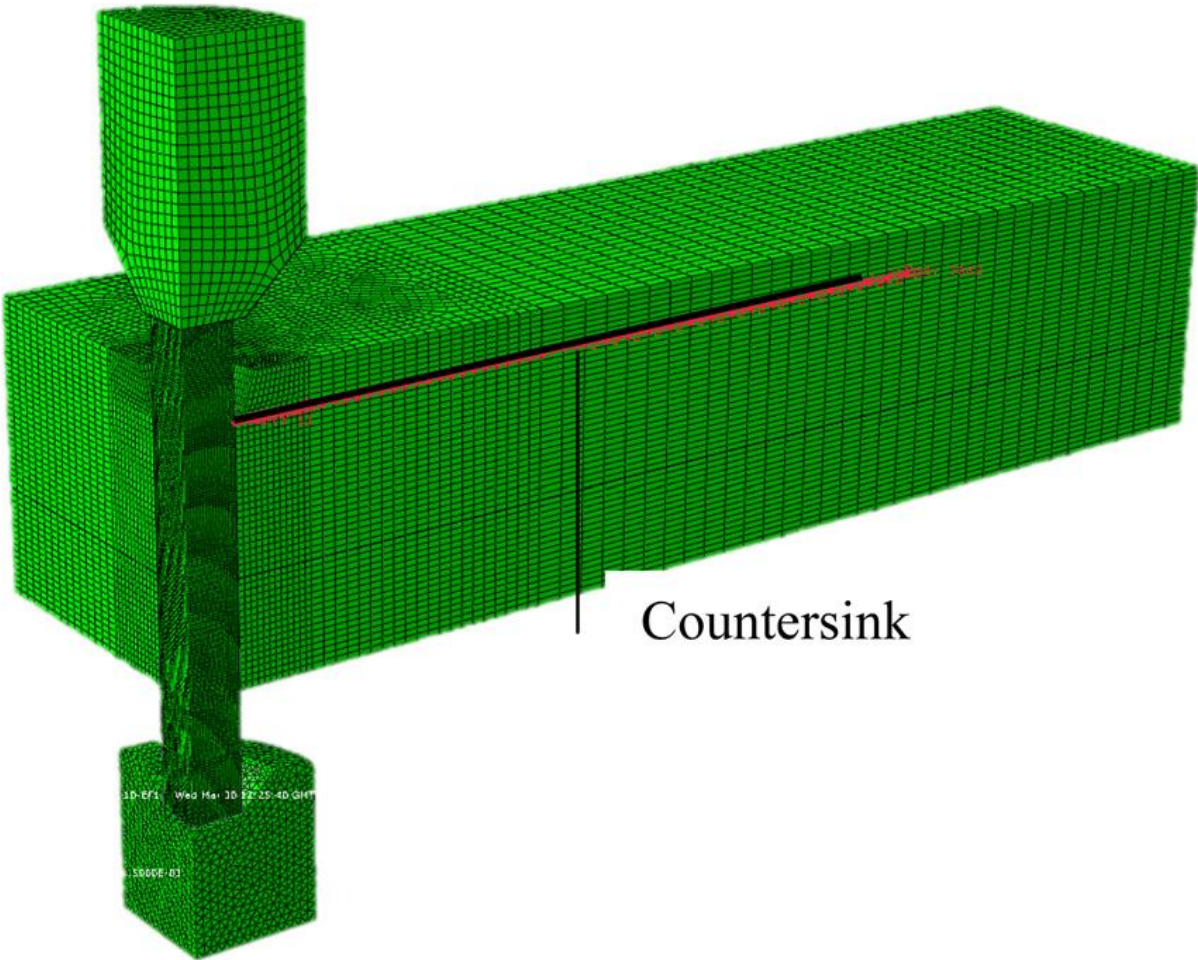
Fig. 6   Nonlinear finite element model for simulating single rivet insertion with alternative head_die designs

(a)

(b)
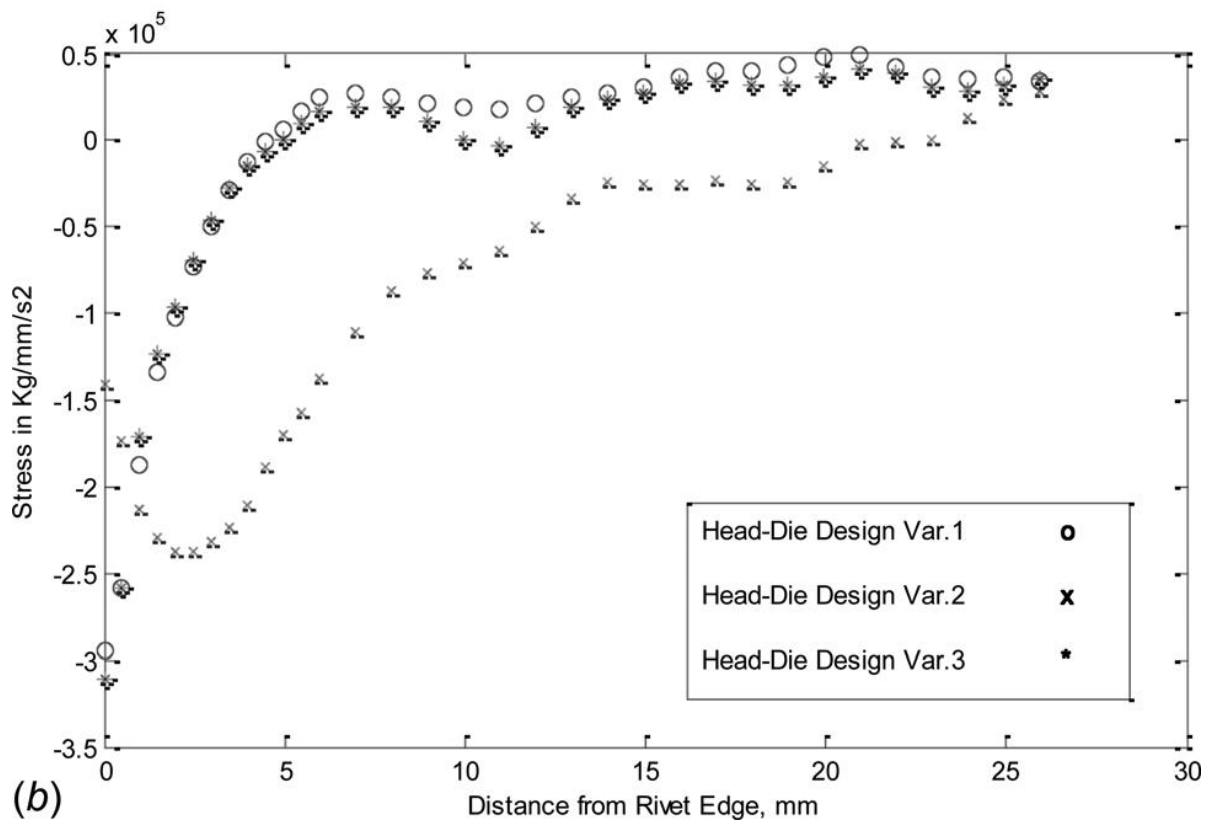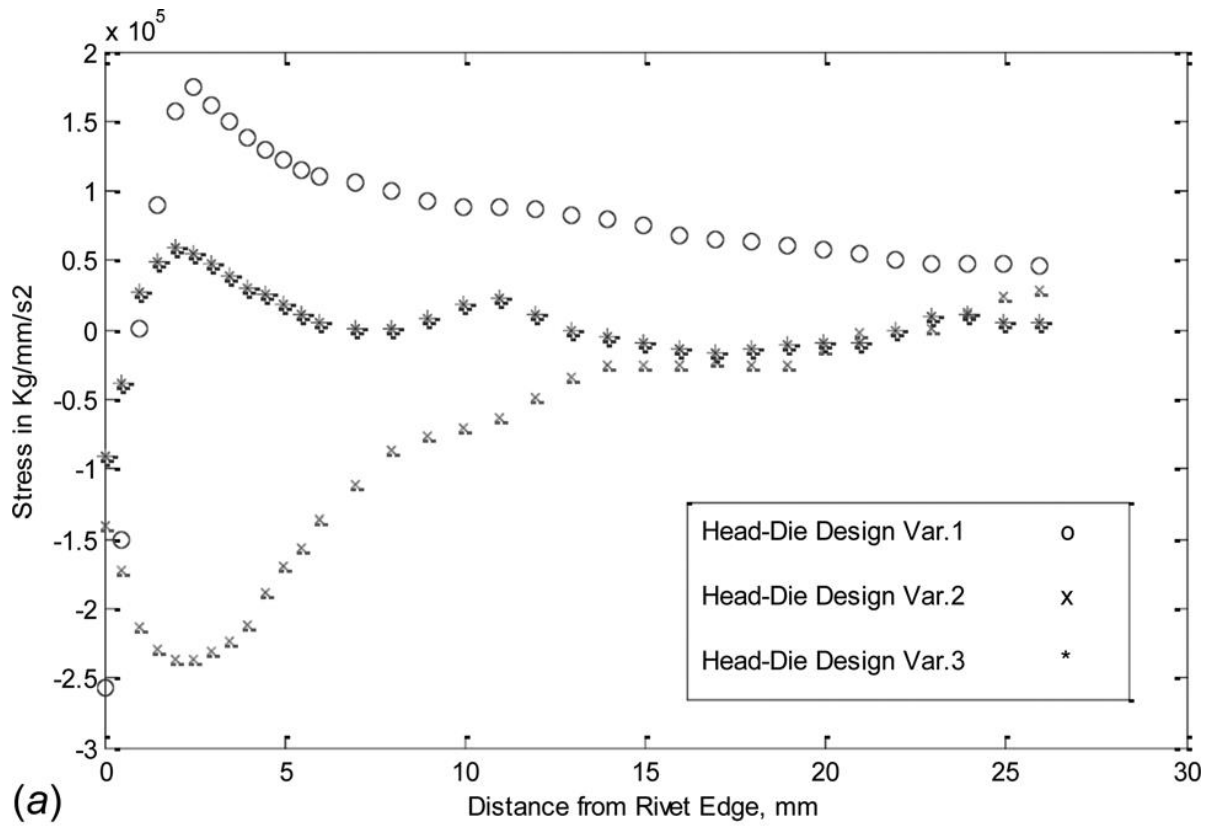
Fig. 7 (a) Residual tangential stresses along the countersink line for three alternative head die designs.
(b) Residual radial stresses along countersink line for three alternative head die designs.
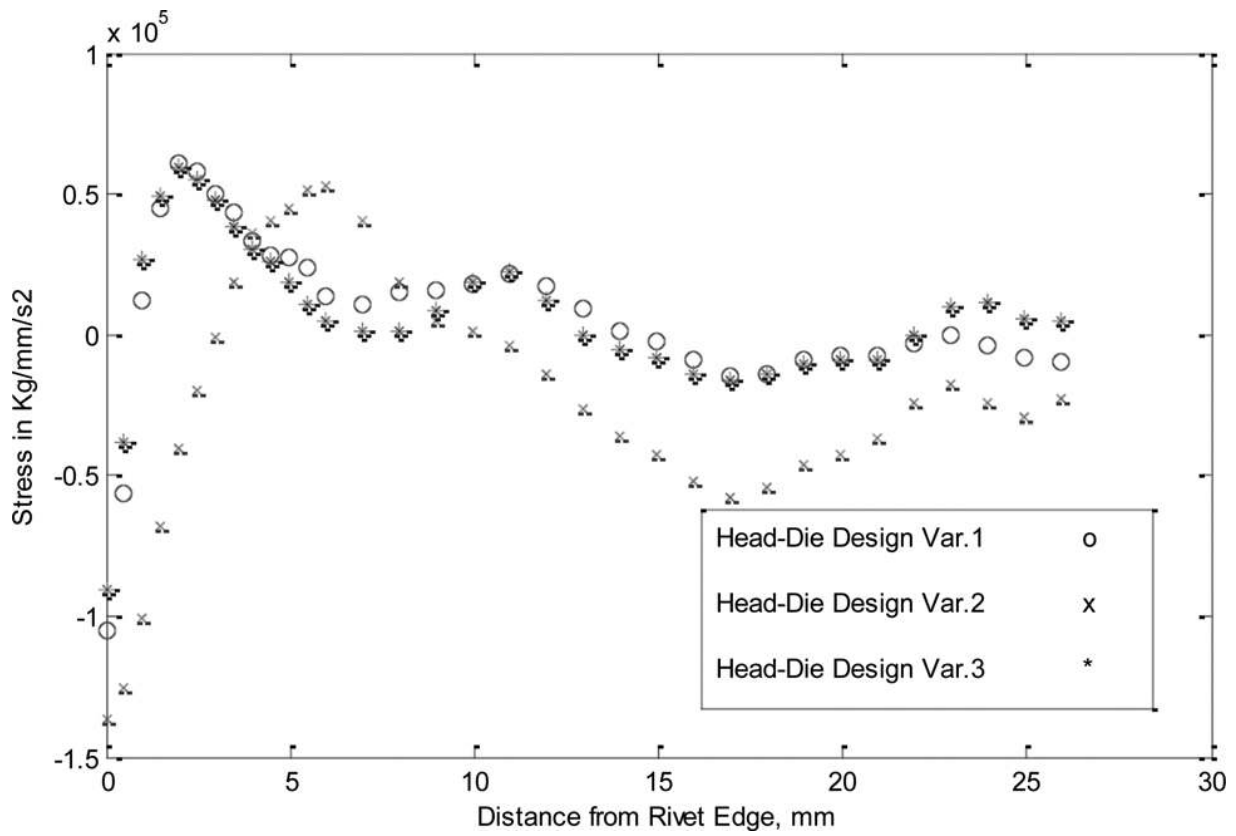
Fig. 8 Normal stresses along countersink line for three alternative head die designs
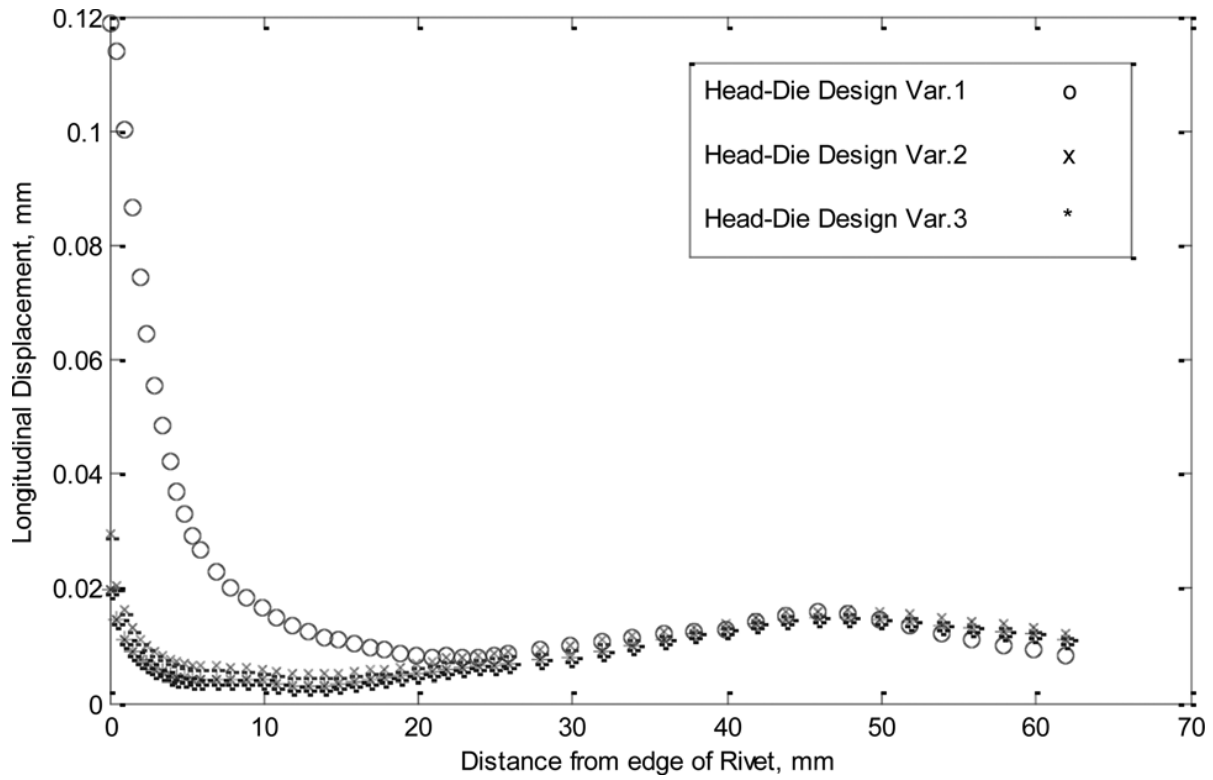
Fig. 9 Displacement wave along countersink line for three alternative head die designs
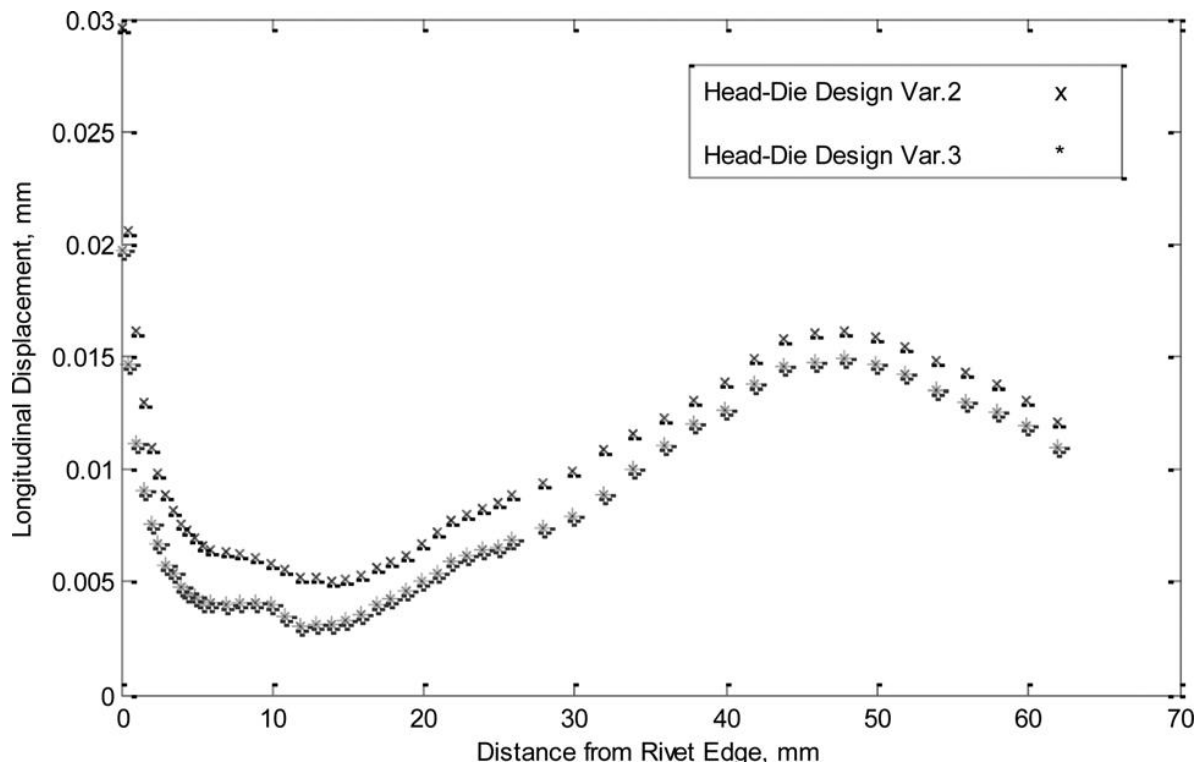
Fig. 10   Displacement wave along the countersink line for two alternative head die designs
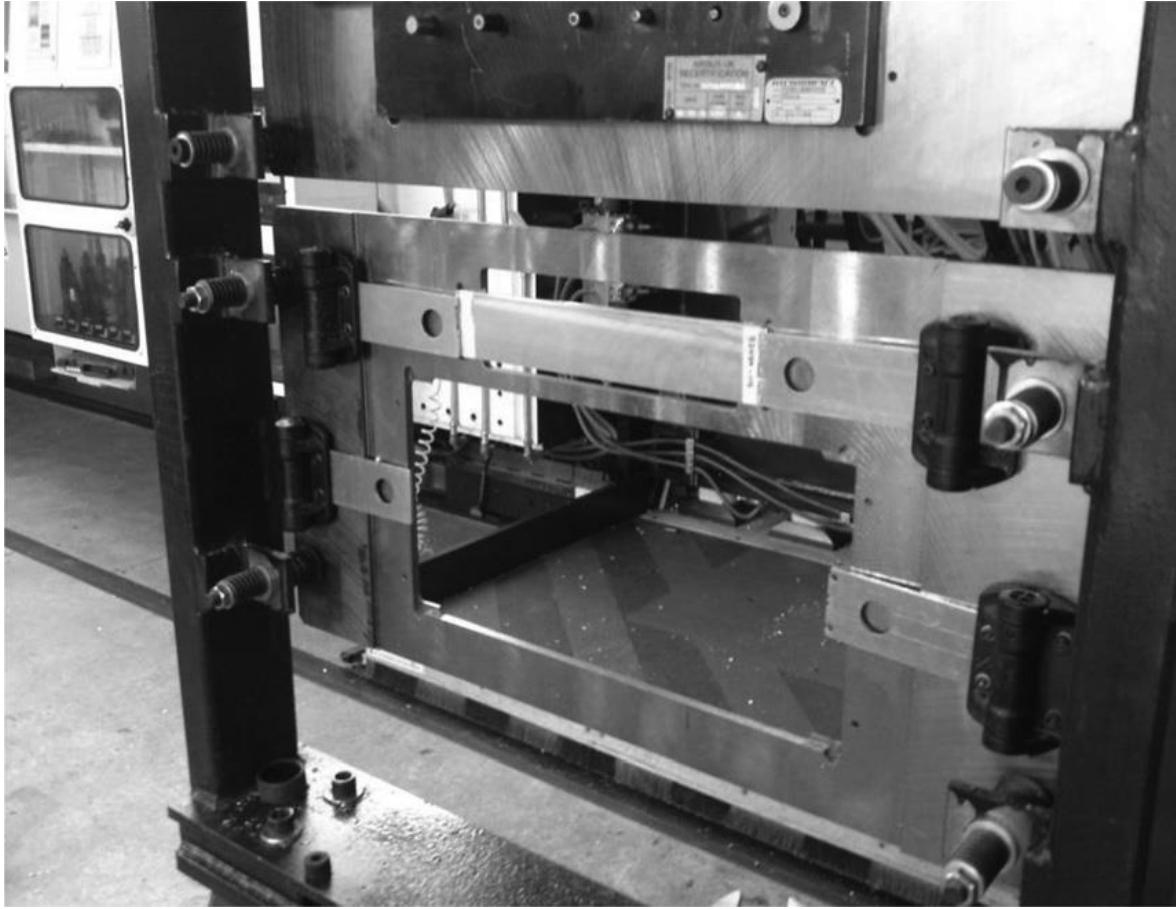
Fig. 11 Customized holding fixture for riveting small panels
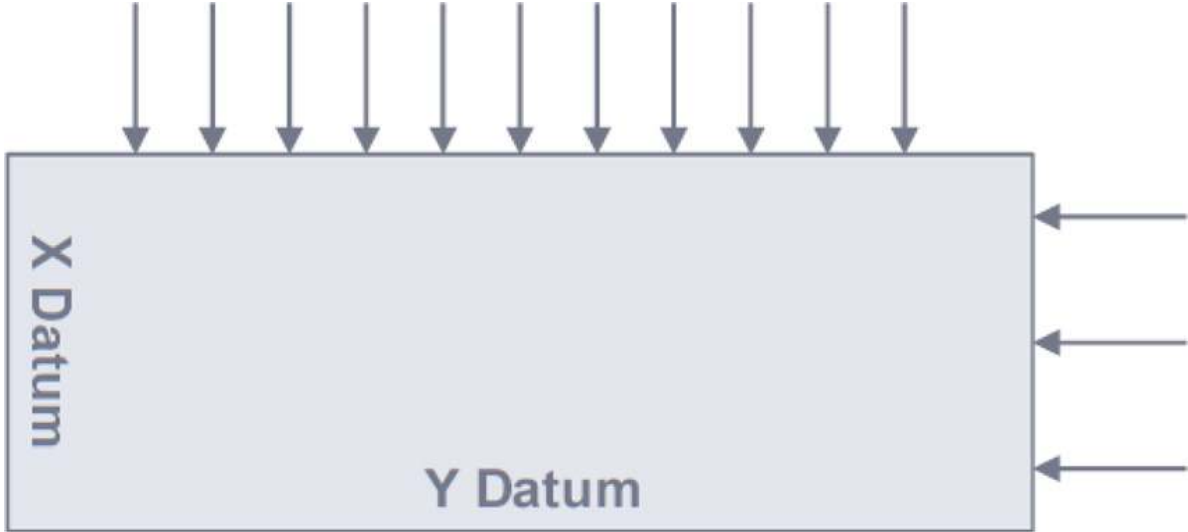
Fig. 12 Measurement locations along the X-axis and Y-axis
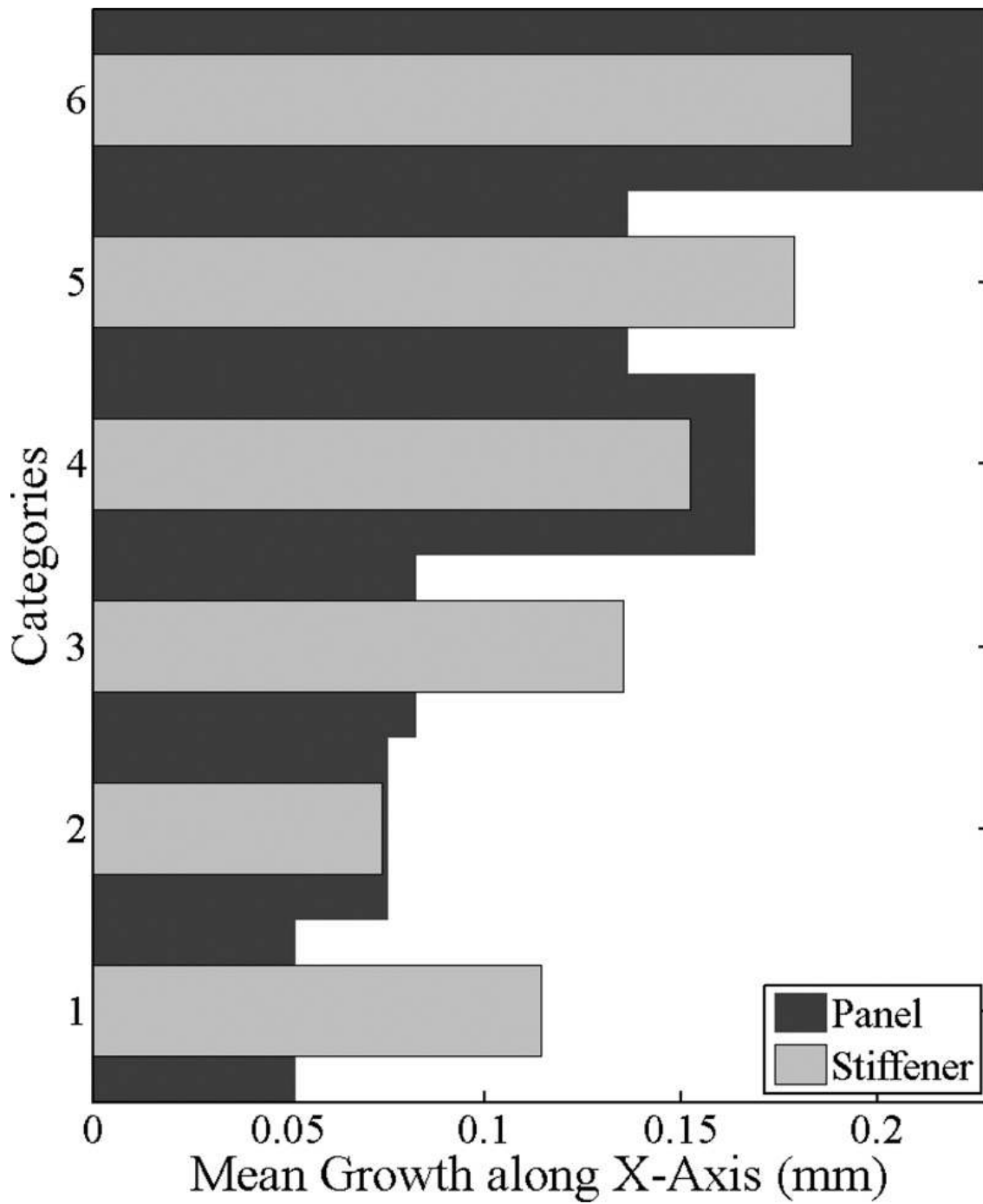
Fig. 13   Mean growth of the small panel assemblies along the X-axis
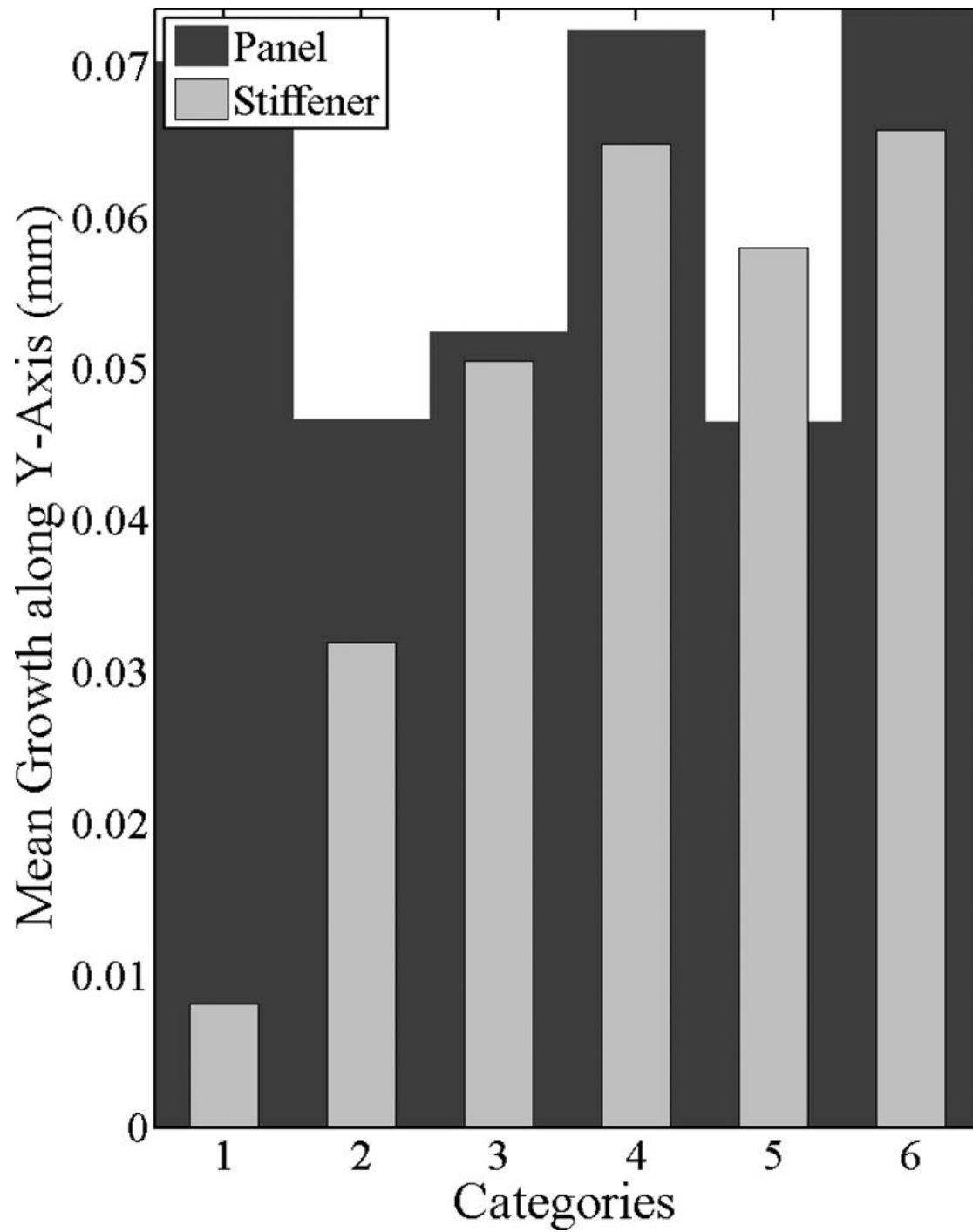
Fig. 14   Mean growth of the small panel assemblies along the Y-axis
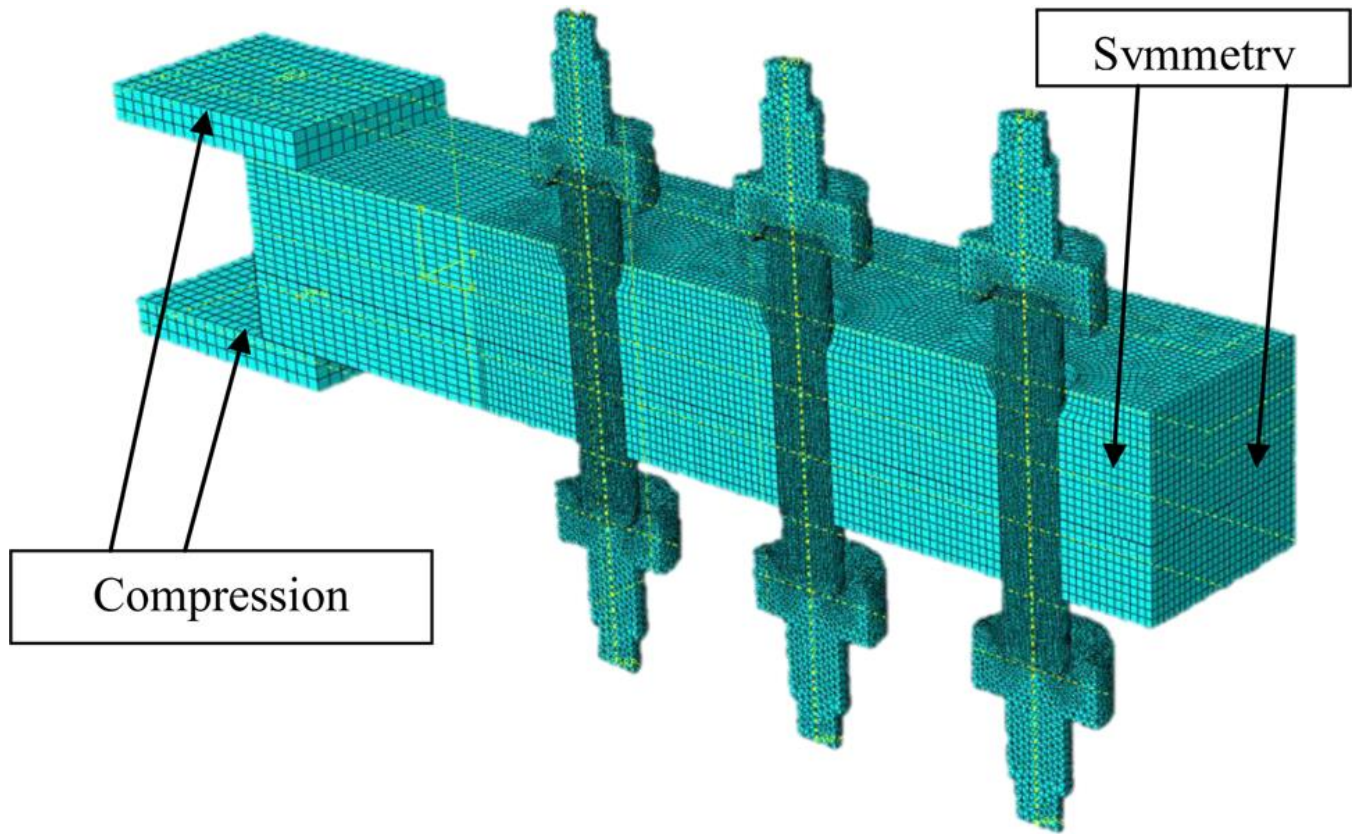
Fig. 15 Nonlinear finite element model for simulating the insertion of rivets on small panel assembly (type 1)
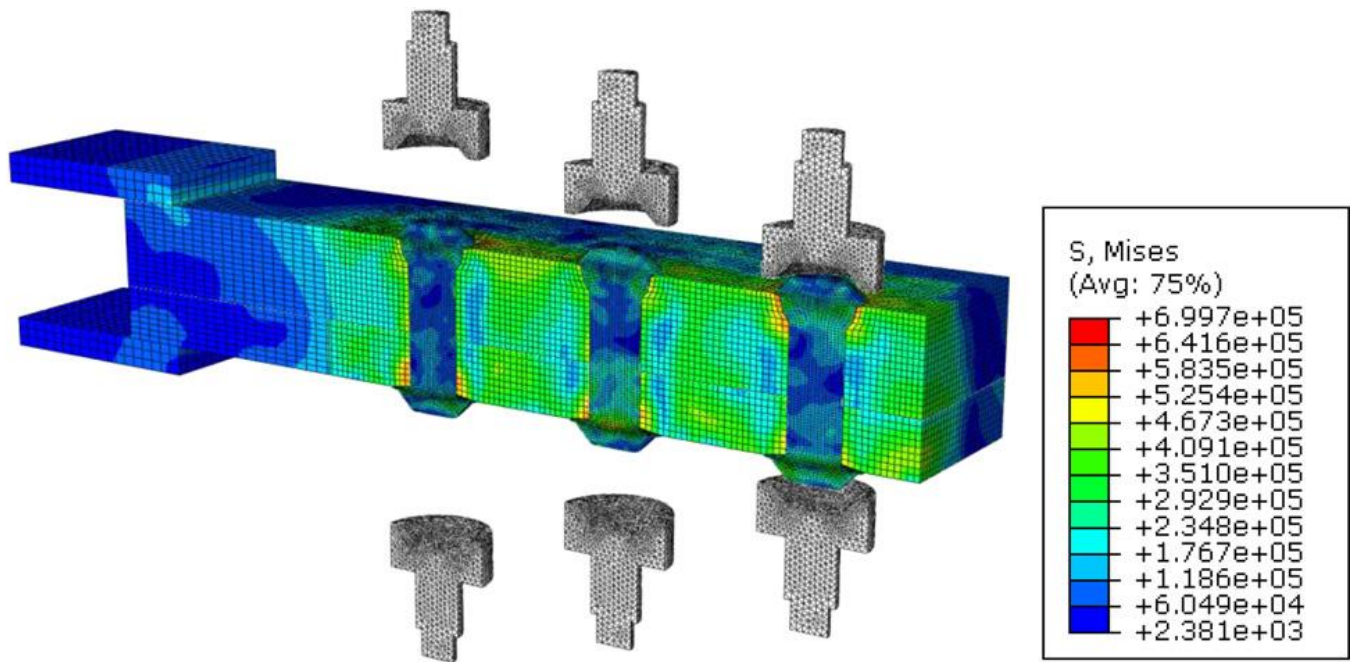
Fig. 16 Deformed small panel assembly after the rivet insertion process. Stress (MPa x 10^{-3})
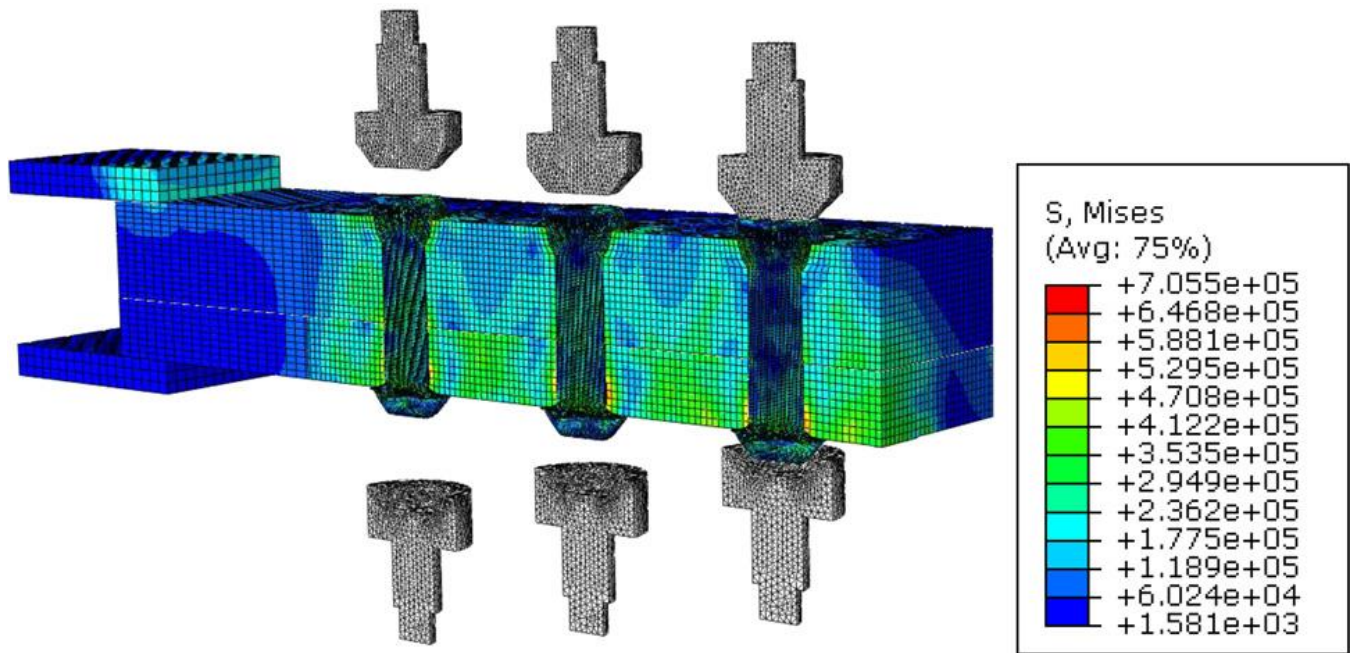
Fig. 17 Deformed panel assembly after the rivet insertion process for an alternative head die design. Stress (MPa x 10^{-3})
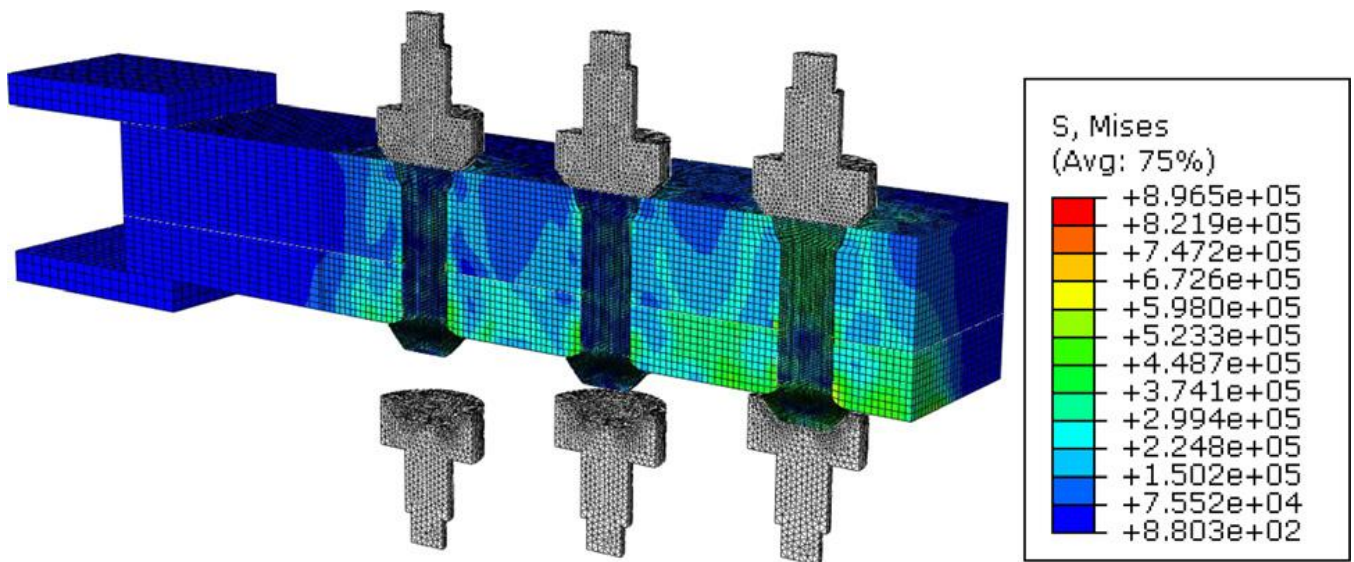
Fig. 18 An alternative riveting process with fixed head of the rivets. Stress (MPa x 10^{-3})
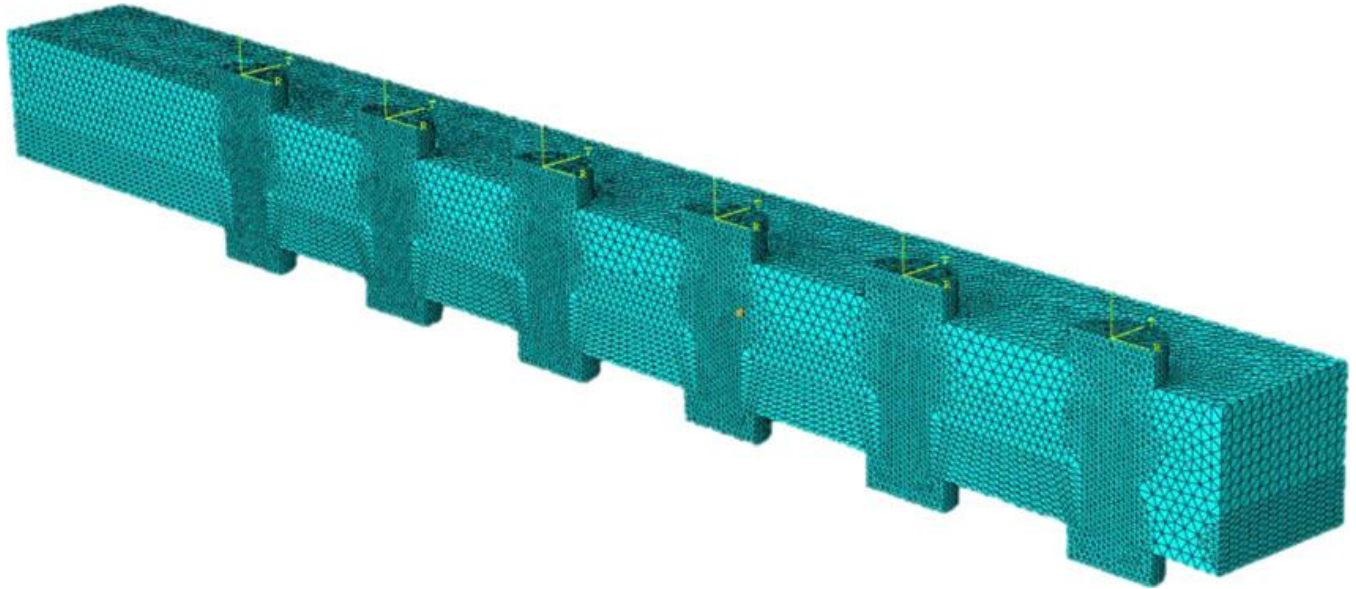
Fig. 19   Finite element model of the small panel assembly (type 1) with minimum allowable rivet pitch distance
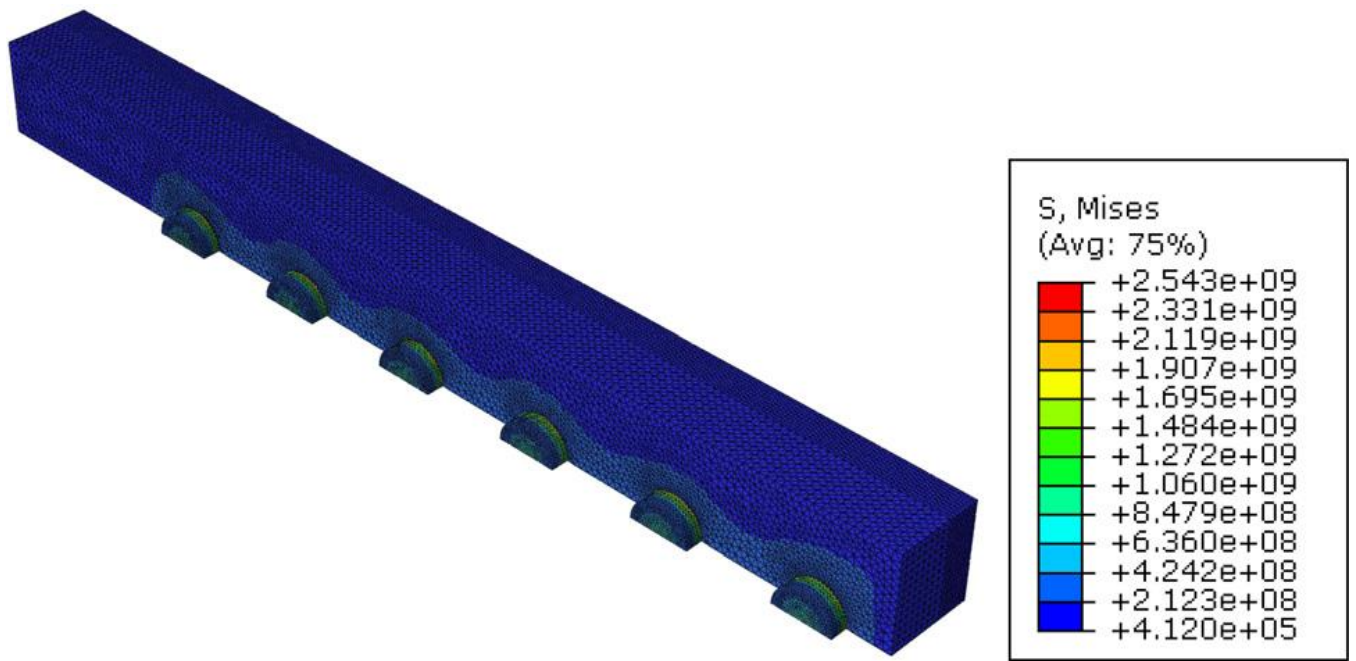
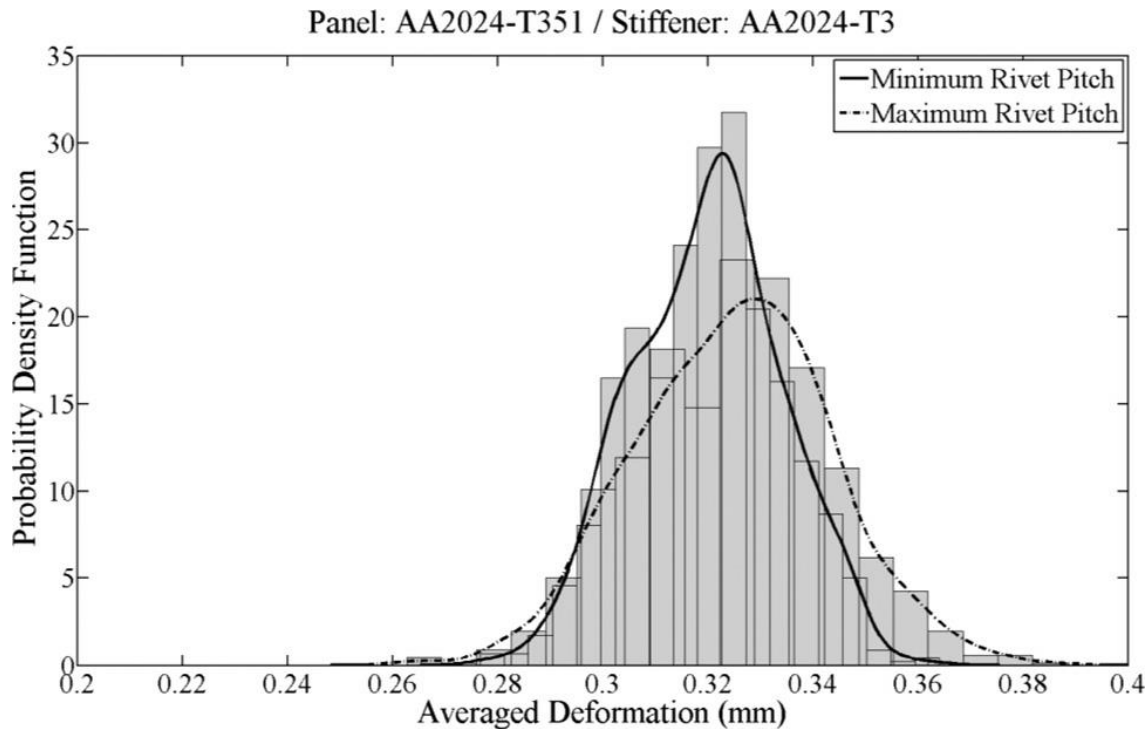Fig. 20 Von Mises stress distribution on small experimental panel (type 1) with minimum rivet pitch distance due to the riveting process; Stress (Pa)

Fig. 21 Probability density function for small panel assembly (type 1), AA2024 (T351-T3) material type and minimum/maximum rivet pitch distances
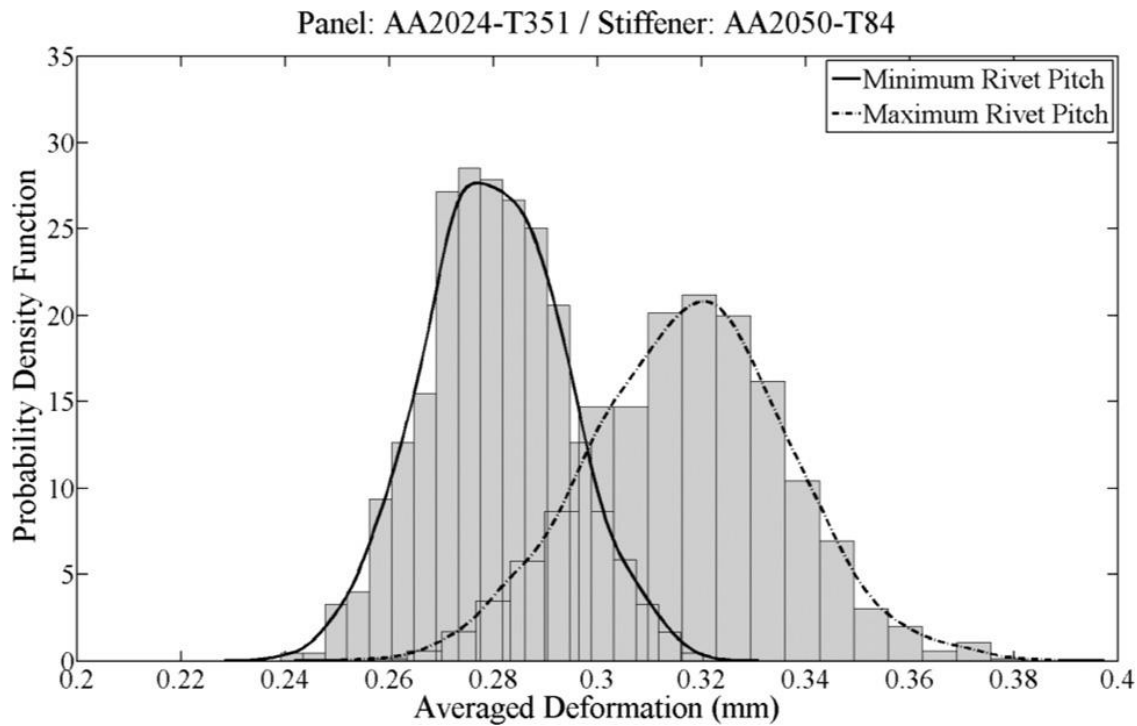

Fig. 22 Probability density function for small panel assembly (type 1), AA2024-AA2050 material type and minimum/maximum rivet pitch distances
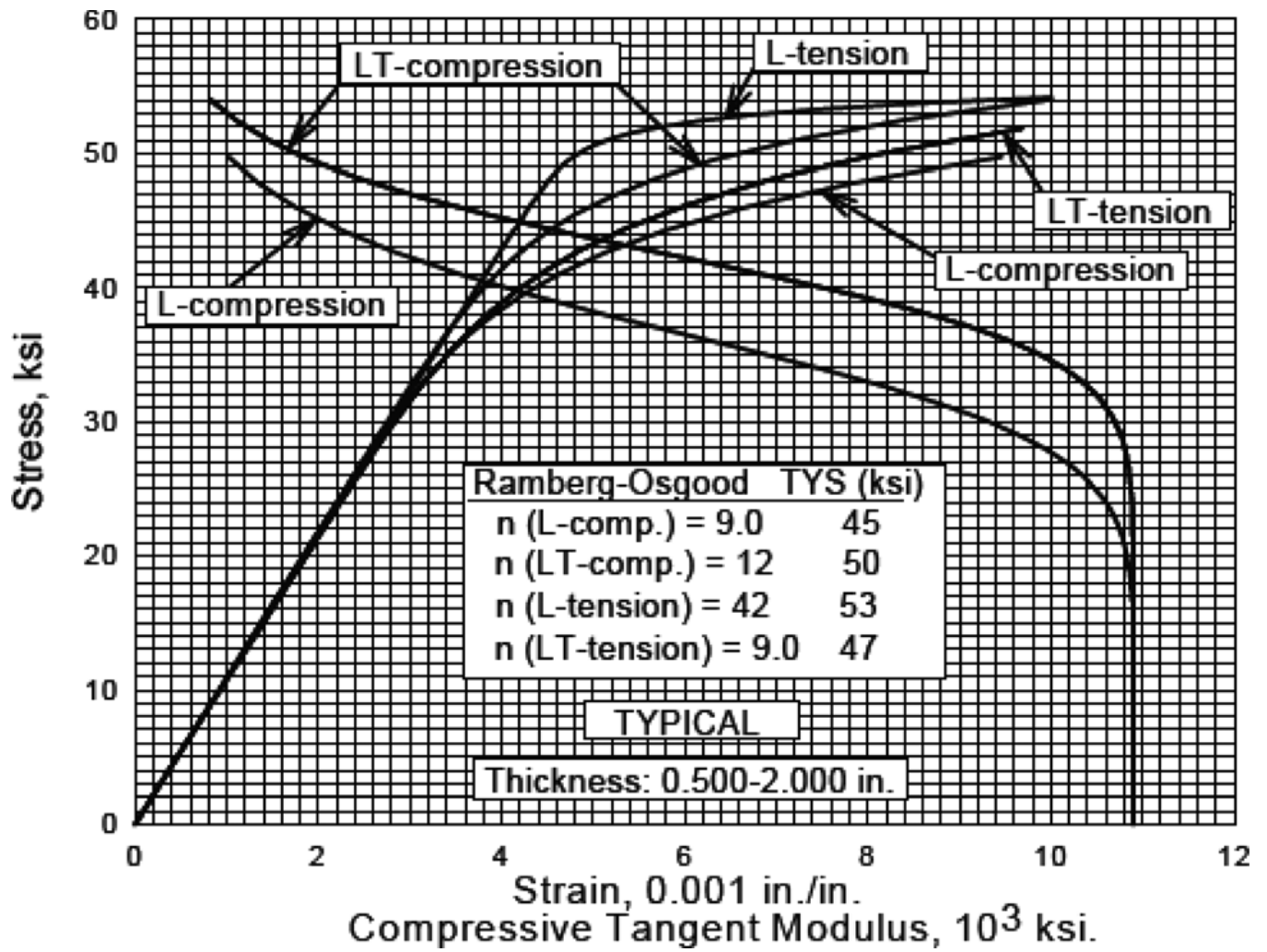
Fig. 23 Typical tensile and compressive stress–strain curves for 2024-T351 aluminum alloy plate at room temperature [21]
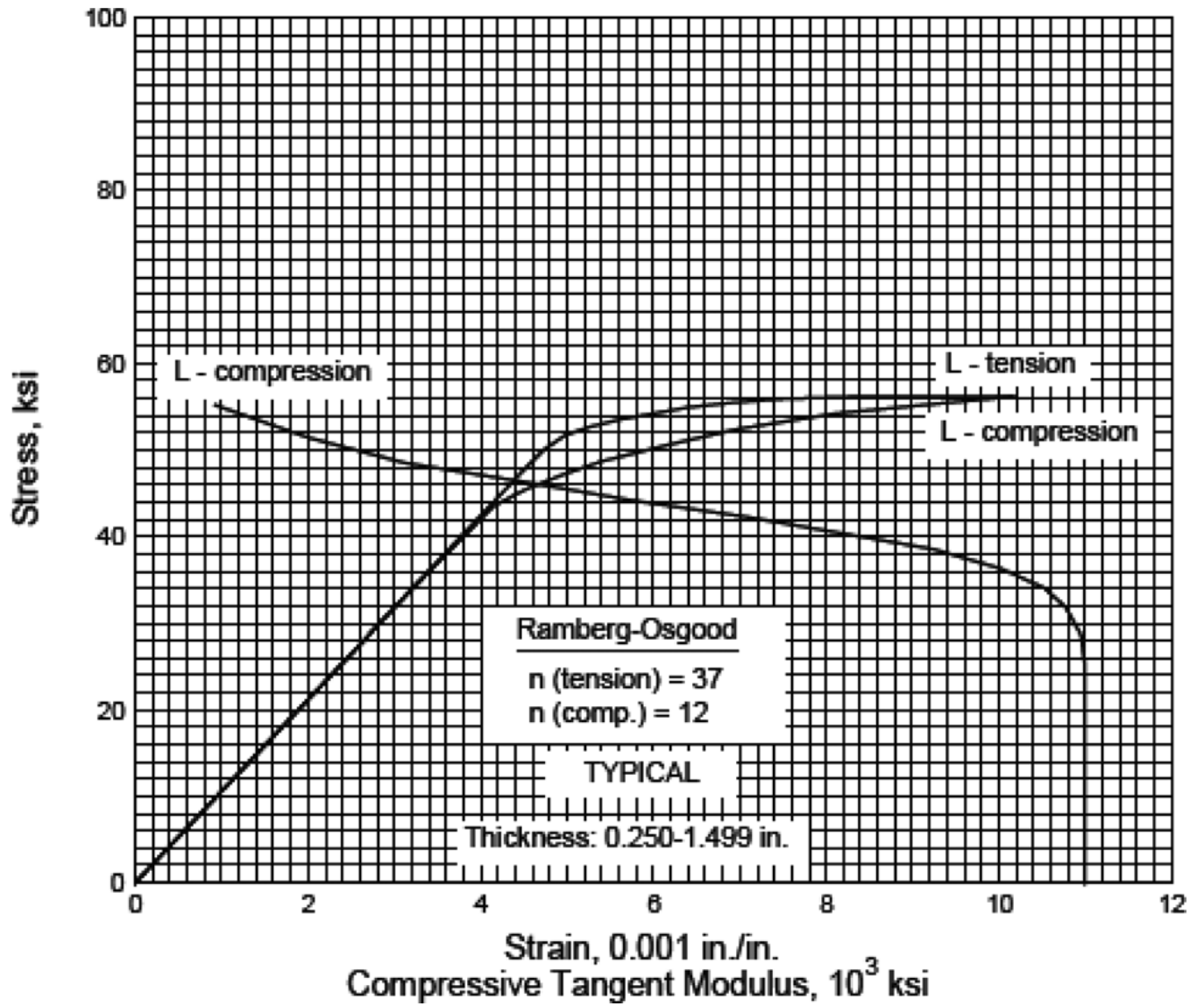
Fig. 24 Typical tensile and compressive stress–strain curves for 2024-T3 aluminum alloy extrusion at room temperature [22]